Inert and seed-competent tau monomers elucidate the structural origins of aggregation

Hilda Mirbaha[1], Olga A. Morozova[2], Kiersten M. Ruff[3], Apurwa Sharma[1], Rohit V. Pappu[3], David W. Colby[2], Hamid Mirzaei[4], Lukasz A. Joachimiak[1], Marc I. Diamond[1]

[1]Center for Alzheimer's and Neurodegenerative Diseases, University of Texas, Southwestern Medical Center, Dallas, Texas 75390

[2]Department of Chemical and Biomolecular Engineering, University of Delaware, Newark, Delaware 19716

[3]Department of Biomedical Engineering, Washington University in St. Louis, St. Louis, Missouri 63130

[4]Department of Biochemistry, University of Texas, Southwestern Medical Center, Dallas, Texas 75390

Corresponding Author
Marc I. Diamond, M.D.
NL10.120
5323 Harry Hines Blvd.
Dallas, TX 75390

Email: marc.diamond@utsouthwestern.edu
Phone: 214-648-8857

Abstract

Tauopathies are defined by progressive accumulation of tau amyloids. These assemble around a protein seed, whose structure is unknown, but might explain the initiation of pathology. We have purified and characterized distinct forms of tau monomer—either seed-competent or inert. Recombinant tau that was seed-competent triggered intracellular tau aggregation, induced full length tau fibrillization *in vitro*, and exhibited intrinsic properties of self-assembly. Tau monomer from AD brain, but not from controls, similarly seeded aggregation, and self-assembled *in vitro* to form higher order, seed-competent structures. We used crosslinking with mass spectrometry to identify distinct conformers of both recombinant tau and human brain-derived protein. Theoretical models informed by this data suggest that VQIINK and VQIVYK sequences, which support amyloid formation, are uniquely exposed in all seed-competent structures. Our data imply that initiation of pathological aggregation begins with conversion of tau monomer from an inert to a seed-competent form.

Introduction

Amyloids are ordered protein assemblies, typically rich in beta sheet, that underlie multiple disorders including Alzheimer's disease (AD). Amyloid-forming proteins include tau, synuclein, and expanded polyglutamine proteins such as huntingtin, among many others. It is unknown how or why intracellular amyloid proteins such as tau transition from a relatively inert form to one that efficiently self-assembles into ordered structures. This process begins with the formation of a pathogenic "seed," a structure that serves as a template for homotypic fibril growth. This structural transition could be the critical event in the pathogenesis of neurodegeneration. Under defined conditions and relatively high concentrations (typically micromolar), recombinant tau monomer will form amyloid fibrils *in vitro*. However free monomer in cells is likely at a much lower concentration, and a complex intracellular protein milieu, with competing heterotypic interactions, theoretically should inhibit spontaneous self-assembly. The conversion of a protein from a monomer to a large, ordered multimer may occur by multiple mechanisms, but a proximal step involves the formation of a seed. This event, and indeed the actual form of the protein that constitutes the "minimal" seed, has remained obscure. This has led to the idea that a seed is potentially transitory, arising from equilibrium between two states: one relatively aggregation-resistant, and another that is short-lived. A seed could be a single molecule, or an assembly of molecules. Based on extrapolation from kinetic aggregation studies, it has been suggested that a critical seed for tau and polyglutamine peptide amyloid formation is a single molecule(1,2), while another study has proposed a tau multimer(3). Isolation of the seed-competent form of tau thus could be critical to understanding the initiation of disease.

Tau protein forms amyloids that underlie neurodegeneration in a variety of neuropathological syndromes, collectively termed tauopathies(4). These include AD and frontotemporal dementias, among many others. Multiple groups, including ours, have now observed that tau will propagate an aggregated state from the outside to the inside of a cell, between cells, across synapses, and within brain networks(5). In prior work we used size exclusion chromatography (SEC) to define tau trimers as the minimal unit of spontaneous cellular uptake and intracellular amyloid formation, and proposed this as the smallest particle capable of propagating aggregates between cells(6). This work involved application of "naked" protein assemblies derived from recombinant protein or human brain onto cultured "biosensor" HEK293 cells or primary neurons that express a tau aggregation reporter(7,8). These biosensor cells take up tau aggregates via macropinocytosis(9). The aggregates subsequently serve as highly specific templates to trigger intracellular amyloid formation(8,10). We have also determined that preincubation of cationic lipids such as Lipofectamine with tau seeds will directly transduce them into the cell, bypassing the physiologic uptake mechanism(8,11). Lipofectamine-mediated delivery into biosensor cells allows direct quantitation of seed titer for both tau and α-synuclein(9).

Tau is intrinsically disordered upon isolation from bacteria or mammalian cells, and is relatively inert in terms of spontaneous self-assembly. However under various conditions, including exposure to polyanions such as heparin, tau will form aggregates via nucleated self-assembly (12,13). It is unknown how these experimental conditions relate to the initiation of aggregation in human brain. We have now purified various stable forms of full-length tau monomer from recombinant protein and human brain. One type is relatively inert, and is stable for long periods. Another type is "seed-competent," triggers amyloid formation in cells

and *in vitro*, and exhibits intrinsic properties of self-assembly. We have used crosslinking with mass spectrometry (XL-MS) to probe the structures of these molecules and build theoretical structural models. These models imply that differential exposure of hexapeptide motifs previously known to be important for amyloid formation distinguish the two forms of tau. Identification of distinct and stable forms of tau monomer, including structural isoforms that are uniquely seed-competent, bears directly on how we understand the initiation of protein aggregation in the tauopathies.

MATERIALS AND METHODS

Tau expression, purification, fibrillization, and labeling

We utilized several forms of recombinant tau. Full-length (FL), wild-type (WT) tau contains two cysteines that create disulfide bridges, and complicate isolation of monomer. Thus in addition to preparing FL WT tau (2N4R), we created FL tau (2N4R) that contains two cysteine/alanine substitutions (C291A, C322A), termed tau (2A), and prepared recombinant protein as previously described(14). Additionally, for fluorescence correlation spectroscopy (FCS), we engineered a single cysteine at the amino terminus of this construct (Cys-Tau (2A)) for labeling via sulfhydryl chemistry. These modified proteins have fibrillization and seeding properties similar to FL WT tau. To initiate fibrillization, we incubated tau in 10 mM HEPES, 100 mM NaCl, and 8 μM heparin (1:1 ratio of FL tau to heparin) at 37°C for 72 h without agitation. For cysteine labeling, we incubated 200 μL of 8 μM fibrils (monomer equivalent) and monomer with 0.025 mg of Alexa Fluor-488 (AF488) C5-maleimide (Invitrogen) and 80μM Tetramethylrhodamine-5-maleimide (Sigma-Aldrich) overnight at 4°C with gentle rotation. We quenched excess dye with 10mM DTT for 1h at room temperature. We employ the following terminology to refer to four types of recombinant tau monomer, each comprised of identical primary amino acid (aa) sequences:

M_r: recombinant tau prepared from E. coli, without any further modification or size fractionation.

M_h: recombinant tau treated with heparin for 1min.

M_i: recombinant tau, subsequently isolated by SEC.

M_s: recombinant tau, treated with heparin, allowed to form fibrils, then sonicated, and isolated by SEC.

Sonication and size exclusion chromatography (SEC)

We sonicated labeled and non-labeled fibrils using a Q700 Sonicator (QSonica) at a power of 100-110 watt (Amplitude 50) at 4°C for 3h. Samples were then centrifuged at 10,000 x g for 10 min and 1 mL of supernatant was loaded into a Superdex 200 Increase 10/300 GL column (GE Healthcare) and eluted in PBS buffer at 4°C. After measuring the protein content of each fraction with a Micro BCA assay (Thermo Scientific) and/or fluorescence using a plate reader (Tecan M1000), we aliquoted and stored samples at -80°C until further use. Each aliquot was thawed immediately before use. The molecular weight of proteins in each fraction was estimated by running gel filtration standards (Bio-Rad): Thyroglobulin (bovine) 670 kDa; γ-globulin (bovine) 158 kDa; Ovalbumin (chicken) 44 kDa; myoglobin (horse) 17 kDa; and vitamin B_{12} 1.35 kDa.

CD spectroscopy

Circular dichroism (CD) measurements were performed at 25°C on a Jasco J-815 spectropolarimeter using a 0.1 cm optical path length. 200µL of 2 µM M_s or M_i monomer was dialyzed onto 10 mM NaP and the spectra were measured at 0.10 nm intervals, with a band width of 1.0 nm, and scan speed of 10 nm/min. The spectrum represents the average of 4 scans in the range of 195 to 250 nm.

Enzyme linked immunosorbent assay

A total tau "sandwich" ELISA was performed similarly to that described previously(15). Antibodies were kindly provided by Dr. Peter Davies (Albert Einstein College of Medicine). 96-well round-bottom plates (Corning) were coated for 48 hours at 4°C with DA-31 (aa 150-190) diluted in sodium bicarbonate buffer (6 µg/mL). Plates were rinsed with PBS 3 times, blocked for 2 hours at room temperature with Starting Block (Pierce), and rinsed with PBS 5 additional times. SEC fractions were diluted in SuperBlock solution (Pierce; 20% SuperBlock, diluted in TBS), and 50 µL sample was added per well. DA-9 (aa 102-150) was conjugated to HRP using the Lighting-Link HRP Conjugation Kit (Innova Biosciences), diluted 1:50 in SuperBlock solution, and 50µL was added per well (15µg/mL). Sample + detection antibody complexes were incubated overnight at 4°C. Plates were washed with PBS 9 times with a 15 sec incubation between each wash, and 75 µL 1-Step Ultra TMB Substrate Solution (Pierce) was added. Plates were developed for 30min, and the reaction quenched with 2M sulfuric acid. Absorbance was measured at 450nm using an Epoch plate reader (BioTek). Each plate contained a standard curve, and all samples were run in triplicate.

Fluorescence correlation spectroscopy

FCS measurements were conducted on a Confocal/Multiphoton Zeiss LSM780 Inverted microscope (Carl Zeiss-Evotec, Jena, Germany), using a 40X water immersion objective as previously described (16). Fluorescently labeled tau from SEC fractions (in PBS) was excited at 488nm and 561nm for 30sec, recording 10 times(17). The data analysis was performed with Origin 7.0 (OriginLab, Northampton, MA).

Liposome-mediated transduction of tau seeds

Stable cell lines were plated at a density of 35,000 cells per well in a 96-well plate. After 18h, at 60% confluency, cells were transduced with protein seeds. Transduction complexes were made by combining [8.75 µL Opti-MEM (Gibco) +1.25 µL Lipofectamine 2000 (Invitrogen)] with [Opti-MEM + proteopathic seeds] for a total volume of 20µL per well. Liposome preparations were incubated at room temperature for 20min before adding to cells. Cells were incubated with transduction complexes for 24h.

FRET flow cytometry

Cells were harvested with 0.05% trypsin and fixed in 2% paraformaldehyde (Electron Microscopy Services) for 10min, then resuspended in flow cytometry buffer. The MACSQuant VYB (Miltenyi) was used to perform FRET flow cytometry. To measure CFP and FRET, cells were excited with a 405nm laser, and fluorescence was captured with 405/50nm and 525/50nm filters, respectively. To measure YFP, cells were excited with a 488nm laser and fluorescence was captured with a 525/50nm filter. To quantify FRET, we used a gating strategy similar to that previously described(8). The integrated FRET density (IFD), defined as the percentage of FRET-positive cells multiplied by the median fluorescence intensity of FRET-positive cells, was used for all analyses. For each experiment, ~20,000 cells were

analyzed in triplicate. Analysis was performed using FlowJo v10 software (Treestar).

Tau seeding *in vitro*

Recombinant full length (0N4R) tau monomer was purified as previously described(18) at 1mg/mL in BRB80 buffer (80mM PIPES, 1mM MgCl2, 1mM EGTA, pH 6.8 with 0.3M NaCl) and boiled at 100°C for 5min with 25mM β-mercaptoethanol. The tau protein solution was then rapidly diluted 1:5 and cooled to 20°C in PBS, pH 7.4, to a final concentration of 0.2mg/mL of tau and 5mM β-mercaptoethanol. This solution was supplemented with Thioflavin T (ThT) to a final concentration of 20μM and filtered through a sterile 0.2μm filter. Reaction sizes of 195μL were aliquoted from the prepared protein stock and thoroughly mixed with 5μL of each sample at 100nM monomer equivalent, or 5μL of buffer control. For each sample, three different technical replicates were prepared. An opaque 96-well plate was prepared with a 3mm glass bead added to each well to increase agitation. The recombinant tau solution was added to the plate in 200μl reaction volumes. The plate was sealed with sealing tape to prevent evaporation and incubated in the plate reader (SpectraMax M2) at 37°C. ThT fluorescence was monitored over time with excitation and emission filters set to 444nm and 485nm, respectively. Fluorescence readings were taken every 5min, with agitation for 5sec before each reading.

Tau extraction from brain and characterization by SEC

0.5g frontal lobe sections from AD patients and age-matched controls lacking evident tau pathology were gently homogenized at 4°C in 5mL of TBS buffer containing protease inhibitor cocktails (Roche) using a dounce homogenizer. Samples were centrifuged at 21,000 x g for 15 min at 4°C to remove cellular debris. Supernatant was partitioned into aliquots, snap frozen and stored at -80°C. Immunopurification was performed with HJ8.5 at a ratio of 1:50 (1μg mAb per 50μg of total protein), incubating overnight at 4°C while rotating. To each 1mL of mAb/brain homogenate we added 200μL of a 50% slurry protein G-agarose beads (Santa-Cruz). We washed the bead with TBS buffer before overnight incubation at 4°C. We then centrifuged the complexes at 1000 x g for 3min and discarded the supernatant. Beads were washed with Ag/Ab Binding Buffer, pH 8.0 (Thermo Scientific) three times. Tau bound to the beads was eluted in 100 μL low pH elution buffer (Thermo Scientific), incubated at room temperature for 7min, followed by neutralization with 10μL Tris-base pH 8.5. This elution step was repeated once more with 50 μL elution buffer and 5μL Tris-base pH 8.5 for a total of 165μL. Samples were then centrifuged at 10,000 x g for 10min, and the supernatant loaded onto a Superdex 200 Increase 10/300 GL column (GE Healthcare). SEC fractions were frozen at -80°C after evaluation of protein content by Micro BCA assay (Thermo Scientific).

To compare different extraction methods, fresh frozen frontal lobe section from an AD patient was suspended in TBS buffer containing protease inhibitor cocktails (Roche) at 10% w/vol in 4 portions. Samples were homogenized using 3 different devices: a dounce homogenizer, probe sonicator (Omni International), and tissue homogenizer (Power Gen 125, Fischer Scientific). We also included one more condition of homogenizing with tissue homogenizer followed by probe sonication for 10min. Samples were centrifuged at 21,000 x g for 15min at 4°C to remove cellular debris. Supernatant was partitioned into aliquots followed by immunopurification.

Analysis of heat denaturation data

We analyzed the IFD from measurements of temperature dependent seeding using global fits to a proposed unimolecular heat denaturation reaction. This analysis rests on the Arrhenius equation(19):

$$k_U = Ae^{-\frac{E}{RT}}$$

where k_U is the unfolding rate constant, E is the activation energy, R is the gas constant, T is the temperature, and A is the pre-exponential factor. For the unimodal model, the data were fit globally to:

$$\mathrm{IFD}(t) = 100e^{-t/\tau}.$$

Here, t is the heat denaturation time and $\tau = 1/k_U$ is the unfolding time. A second, multimodal model was deployed to account for discrepancies in the early time points which appeared to suggest the presence of a lag phase in denaturation. In this model, the data were fit globally to

$$\mathrm{IFD}(t) = 100; \qquad t \le l_t$$
$$\mathrm{IFD}(t) = 100e^{-(t-l_t)/\tau}; t > l_t$$

where l_t is the lag time given by

$$1/l_t = Be^{-\frac{E}{RT}}$$

and B is a pre-exponential factor. We used the Akaike information criterion (AIC) to evaluate the best model as it quantifies the trade-off between goodness of fit and the complexity of the model (20). For least squares model fitting, AIC can be reduced to:

$$\mathrm{AIC} = 2p + n\ln(\mathrm{RSS}/n)$$

where p is the number of parameters in the model, n is the number of observations, and RSS is the residual sum of squares. The preferred model is the one with the minimum AIC. Here, we find AIC = 123 for the unimodal model and AIC = 105 for the multimodal model, which suggests the multimodal model is a better description of the denaturation data.

Crosslinking, sample processing and LC-MS/MS analysis

M_i and M_s tau samples were prepared as described above. In all cases, tau preparations were crosslinked at a total protein concentration of ~0.1mg/mL using 10 – 20µg starting material. The crosslinking buffer was 50 mM HEPES-KOH (pH 7.4) containing 300mM NaCl and 1mM DTT. The crosslinking reaction was initiated by adding disuccinimidyl suberate (DSS) stock solution (25 mM DSS-d_0 and $-d_{12}$, Creative Molecules) in DMF to a final concentration of 1 mM. Samples were incubated at 37°C for 1min. For the M_h sample, heparin sulfate (Sigma) was added to a final concentration of 5µM, followed by 1mM DSS and the samples were inclubated for 1min at 37°C. Excess reagent was quenched by addition of ammonium hydrogen carbonate to 50mM and incubation at 37°C for 30min, and then flash frozen at -80°C. After the quenching step, samples were evaporated to dryness in a vacuum centrifuge and resuspended in 8M urea. Proteins were reduced with 2.5mM TCEP (37°C, 30 min) and alkylated with 5mM iodoacetamide (30min, room temperature, protected from light). The sample solutions were diluted to 1M urea with 50mM ammonium hydrogen carbonate and trypsin (Promega) was added at an enzyme-to-substrate ratio of 1:50. Proteolysis was carried out at 37°C overnight followed by acidification with formic acid to 2%

(v/v). Samples were then purified by solid-phase extraction using Sep-Pak tC18 cartridges (Waters) according to standard protocols. Samples were fractionated by size exclusion chromatography (SEC) on a Superdex Peptide column as described elsewhere (21). Two fractions collected from SEC were evaporated to dryness and reconstituted in water/acetonitrile/formic acid (95:5:0.1, v/v/v) to a final concentration of approximately 0.5 µg/µl. 2µL each were injected for duplicate LC-MS/MS analyses on an Eksigent 1D-NanoLC-Ultra HPLC system coupled to a Thermo Orbitrap Fusion Tribrid system. Peptides were separated on self-packed New Objective PicoFrit columns (11cm x 0.075mm I.D.) containing Magic C_{18} material (Michrom, 3µm particle size, 200Å pore size) at a flow rate of 300nL/min using the following gradient. 0-5min = 5 %B, 5-95min = 5-35 %B, 95-97min = 35-95 %B and 97-107min = 95 %B, where A = (water/acetonitrile/formic acid, 97:3:0.1) and B = (acetonitrile/water/formic acid, 97:3:0.1). The mass spectrometer was operated in data-dependent mode by selecting the five most abundant precursor ions (m/z 350-1600, charge state 3+ and above) from a preview scan and subjecting them to collision-induced dissociation (normalized collision energy = 35%, 30ms activation). Fragment ions were detected at low resolution in the linear ion trap. Dynamic exclusion was enabled (repeat count 1, exclusion duration 30sec).

Analysis of mass spectrometry data

Thermo .raw files were converted into the open .mzXML format using msconvert (proteowizard.sourceforge.net) and analyzed using an in-house version of xQuest(22). Spectral pairs with a precursor mass difference of 12.075321 Da were extracted and searched against the respective FASTA databases containing Tau (TAU_HUMAN P10636-8). xQuest settings were as follows: Maximum number of missed cleavages (excluding the crosslinking site) = 2, peptide length = 5-50 aa, fixed modifications = carbamidomethyl-Cys (mass shift = 57.021460 Da), mass shift of the light crosslinker = 138.068080 Da, mass shift of mono-links = 156.078644 and 155.096428 Da, MS^1 tolerance = 10 ppm, MS^2 tolerance = 0.2 Da for common ions and 0.3 Da for crosslink ions, search in ion-tag mode. For brain derived samples we also included variable modifications including: Methionine oxidation = 15.99491, Ser/Thr/Tyr Phosphorylation = 79.96633 and Lysine Ubiquitylation = 114.043 with nvariable_mod = 1. Post-search manual validation and filtering was performed using the following criteria: xQuest score > 7, mass error between -4 and +7ppm, %TIC > 10, and a minimum peptide length of six aa. In addition, at least four assigned fragment ions (or at least three contiguous fragments) were required on each of the two peptides in a crosslink. False discovery rates for the identified crosslinks were estimated using xprophet(22). Crosslink data was visualized using Xvis(23).

Generation of structural models using XL-MS-derived constraints

High confidence crosslink pairs identified above were used to generate an ensemble of possible structures using a Rosetta protocol employing the crosslink pairs as structural restraints. The integration of XL-MS derived restraints have been previously used to refine structural models of large complexes(21) and simpler heterodimeric complexes(24). Based on distance distributions of crosslink pairs mapped onto crystallographic structures we set a lower bound of 15Å and an upper bound of 25Å for lysine Cα pairs in our simulations. Importantly, in our simulations we weighted the constraint pairs as to allow some distances above the upper bound limit. The fragment library was supplanted by using chemical shifts derived from tau (bmrb entry 17920) using csrosetta(25). We generated 1000 models for each of the four XL-MS datasets on a high performance cluster (biohpc.swmed.edu).

Because crosslinks were absent in the N- and C-termini we selected models that excluded additional contacts from residues 1-150 and 400-441. Low energy structures with radius of gyration$_{FL/Frag}$ ratios >2 and contact order $_{FL/Frag}$ ratios between 0.9 and 1.1 were further analyzed. Relative contact order (i.e. intramolecular crosslink distance) was computed using a perl script and is defined as the average sequence distance between all pairs of contacting residues normalized by the total sequence length. Contact maps were computed using a python script and all figures were generated using Pymol. All plots were generated using gnuplot.

Commandline used for *ab initio* protocol calculations with XL-MS restraints

AbinitioRelax.default.linuxgccrelease -in:file:fasta tau.fasta -file:frag3 tau.frags3.dat -file:frag9 tau.frags9.dat -nstruct 1000 -abinitio::increase_cycles 0.5 -abinitio::relax -score::weights score13_env_hb -abinitio::rg_reweight 0.5 -abinitio::rsd_wt_helix 0.5 -abinitio::rsd_wt_loop 0.5 -disable_co_filter true -out:file:silent csrosetta.out -constraints:cst_fa_file tau.cst -constraints:cst_file tau.cst -constraints:cst_weight 0.1 -constraints:cst_fa_weight 0.1 -loopfcst::coord_cst_weight 10.0

Statistical analysis

Group mean values were analyzed by one-way ANOVA with Bonferroni post hoc significant differences test using GraphPad prism 5 software. Data in text and figures are represented as mean ± SEM.

RESULTS

Isolation of monomer from unfibrillized or fibrillized sources

We initially sought to define the tau seeding unit that would trigger intracellular aggregation upon direct delivery to the cell interior. We had previously observed that a tau trimer is the minimal assembly size that triggers endocytosis and intracellular seeding(6). These experiments depended on spontaneous cell uptake, since no Lipofectamine was added to the reactions. A prior study had also indicated the role of disulfide linkages in promoting tau aggregation, potentially by dimer formation(3). Thus, for our initial studies we engineered and purified full-length (FL) tau monomer that lacks any internal cysteines due to alanine substitution (C299A and C322A), termed tau (2A). FL tau (2A) cannot self-associate based on disulfide linkages, which helped prevent the formation of cryptic dimers that could confound our studies. These substitutions do not affect tau purification, heparin-induced fibrillization, and sonication protocols, which we performed as described previously(6). We covalently labeled the fibril preps prior to sonication and isolation of recombinant FL tau (2A) assemblies of various sizes by size exclusion chromatography (SEC)(6). In parallel, we also studied FL wild type (WT) tau. We used methods identical to those described previously, which included controls of fluorescence correlation spectroscopy (FCS), and crosslinking to confirm purification of *bona fide* monomer(6). We purified unfibrillized recombinant FL tau (2A) monomer by SEC (Fig. 1A), and isolated SEC fractions of sonicated fibrils that contained putative monomer, dimer, trimer and ~10-mer (Fig. 1B).

Fibril-derived monomer exhibits seeding activity in cells and *in vitro*

To test the seeding activity of the tau preparations, we used a previously described "biosensor" cell reporter line(8).These cells stably express 4R tau repeat domain (RD)

containing the disease-associated P301S mutation fused to cyan and yellow fluorescent proteins (tau-CFP/YFP). Exogenously applied seeds induce intracellular aggregation with resultant fluorescence resonance energy transfer (FRET) measured via flow cytometry(8,11). The degree of aggregation is scored using "integrated FRET density" (IFD), which is the product of the percent positive cells and the mean fluorescence intensity of FRET-positive cells, and from this we determine a titer of tau seeding activity(8). Lipofectamine directly transduces tau assemblies across the plasma membrane and increases the assay's sensitivity by approximately 100-fold. Upon incubation with Lipofectamine, we readily observed seeding by larger assemblies, whether FL WT or 2A. Surprisingly, we also observed seeding activity in the monomer fractions (Fig. 1C). There was no difference between FL WT tau, and FL tau (2A) (Fig. 1C). We termed the inert monomer "M_i," and the seed-competent monomer "M_s." We confirmed our observations using epifluorescence microscopy, which revealed induction of intracellular inclusions after exposure of cells to M_s, but not M_i (Fig. 1D). These surprising results inspired us to check whether heparin itself could lead to the formation of a seed-competent monomer. We exposed FL WT tau to heparin for varying amounts of time, before purifying different assembly sizes by SEC and testing for seeding activity. After 15min of heparin exposure, we detected low but significant amounts of seed-competent monomer, while larger assemblies were more rare (Fig. 1E). Recombinant monomer not treated with heparin had no seeding activity at any time point (Fig. 1E). At later time points (1h, 4h) monomer fractions as well as larger assemblies all had strong seeding activity (Fig. 1E). To rule out an artifact of the Lipofectamine transduction, we tested FL (2A) tau preparations in an *in vitro* seeding assay that induces fibril formation by full-length tau (0N4R) through iterative polymerization and agitation steps(18). M_i had no intrinsic seeding activity. However M_s induced amyloid formation, albeit more slowly than trimer or unfractionated fibrils (Fig. 1F). We concluded that the M_s fraction contains seeding activity that enables intracellular aggregation of tau RD-CFP/YFP in cells, or full-length tau *in vitro*, and that heparin-exposed monomer also developed seeding activity prior to its formation of larger assemblies.

Comparison of M_i and M_s by CD and FCS

We were intrigued to observe seeding activity in a monomer fraction, and thus attempted to detect multimers. To begin, we tested for obvious structural differences between M_i and M_s using CD spectroscopy, which revealed none (Fig. 2A). We confirmed the sizes of species isolated after sonication using FCS, which measures particle diffusion through a fixed volume (Fig. 2B). As we previously observed(6), we accurately estimated the sizes of small assemblies (≤10-mer), but not larger assemblies (>10-mer) (Fig. 2B). Next, we used double-label FCS in an attempt to identify multimers within the M_s fraction. We engineered a cysteine onto the amino terminus of FL tau (2A) to enable covalent modification (Cys-Tau (2A)). We then prepared Cys-tau (2A) fibrils, or monomer, and labeled them simultaneously with Alexa488 (green) and tetramethylrhodamine (TMR, red) via maleimide chemistry. We carried out sonication and purification by SEC as before, isolating assemblies of various sizes. We evaluated each for cross-correlation between red and green signal, which indicates the presence of at least two tau molecules in a particle. We analyzed >300 events for each assembly. When we evaluated M_i and M_s, 100% of events in each case showed a diffusion time consistent with a molecule of ~50kD, which corresponds to the tau monomer (Fig. 2C,D). Furthermore we observed no cross-correlation between red and green signal, indicating that neither preparation had detectable multimeric assemblies (Fig. 2C,D,H). By contrast, when we evaluated larger species such as dimer, trimer, or ~10-mer, we observed longer diffusion times consistent with the predicted assembly sizes, and significant cross-

correlation values (Fig. 2E-H), consistent with the presence of multimers. In summary, we found no evidence of multimers in the M_s fraction using FCS.

SEC preparation efficiently purifies M_s monomer

To test for contamination of the M_s preparation with larger seed-competent assemblies during SEC, we took three approaches. First, we determined what degree of contamination would be required to give a substantial signal. We titrated M_s to determine an EC_{50} of ~10nM (Fig. 3A), and also titrated dimer and trimer into a solution of 100nM M_i (assuming that those species would most likely account for contamination, if there were any)(Fig. 3B). We observed similar seeding efficiencies from dimer and trimer, with an EC_{50} of ~10nM monomer equivalent (Fig. 3B). In our estimation, these data indicated that to account for signal observed in the seeding assay, contamination of an otherwise inert monomer with larger seed-competent assemblies would have to be substantial.

We next tested the ability of SEC to exclude larger seeds from the monomer fraction. We first isolated M_s and larger assemblies from a sonicated fibril preparation. Removing the fraction that contained M_s (B5), we then pooled the remaining fractions, and spiked them with M_i. We re-fractionated the material on SEC to isolate again the monomer in fraction B5 (Fig. 3C). As previously observed, M_s and other fibril-derived assemblies had seeding activity (Fig. 3D). However, in the second case, while we observed seeding activity in larger assemblies, the monomer (which we take to be M_i) re-isolated from a pool of larger fibril-derived assemblies had no seeding activity (Fig. 3E). This confirmed that larger, seed-competent assemblies do not appreciably contaminate the monomer fraction during SEC.

Finally, we used heat-mediated dissociation of oligomeric assemblies to test for the possibility that M_s in fact represented a uniquely compact multimer that somehow purifies as a monomer. We collected M_s by SEC, and heated the sample to 95°C for 3h. We then re-isolated the sample via SEC. We carried out the same procedure with trimer and ~20-mer. In each case, we tested the resultant fractions for seeding activity. In the first instance, after heating we re-isolated M_s purely as monomer that retained its seeding activity (Fig. 3F). The trimer assembly (fraction B8) broke down to smaller assemblies, predominantly monomer, each of which retained seeding activity (Fig. 3G). The ~20-mer (fraction A5) was largely stable following heat treatment, and retained its seeding activity (Fig. 3H). Based on these experiments, we concluded that our purification protocols leave virtually no contamination of M_s by larger assemblies, and that all detectable seeding activity of M_s in fact derives from monomer.

Differential heat lability of tau assemblies

In the preceding experiment M_s retained seeding activity even after 3h at 95°C, a condition sufficient to dissociate trimers. These experiments implied that M_s consists of a surprisingly stable seed-competent structure, largely resistant to heat denaturation. Consequently, we used more nuanced heat denaturation of seeding activity to probe the relative stabilities of M_s, dimer, trimer, and larger assemblies of FL WT tau. We first isolated tau monomer, dimer, trimer, ~10-mer, and ~20-mer on SEC. We then incubated the various assemblies at a range of temperatures (65, 75, 85, 95°C) and times (0, 3, 12, 18, 24, 48, 72h) before measuring seeding activity. Lower temperatures only slightly reduced seeding activity, whereas exposure of M_s, dimer, and trimer to temperatures ≥85°C for 18-24h eliminated most of it (Fig. 4A-D). By contrast, the seeding activities of ~10-mer and ~20-mer were relatively heat-resistant (Fig. 4A-D). This is consistent with our prior observations that tau seeds derived

from cultured cells are resistant to boiling (10). M_s, dimer, and trimer lost seeding activity at roughly the same rate, while larger assemblies remained intact. To determine a putative energy barrier between M_s and an inert form, we evaluated the denaturation data for M_s, comparing two models for the transition of M_s to an inert form (which we assumed to be an unfolding reaction): a unimodal unfolding model vs. a multimodal model that assumes intermediate seed-competent states. The unimodal model did not account for the data at early time points, which indicated a lag phase in denaturation, whereas the multimodel model performed better (Fig. 4E). The lag phase in denaturation implies an ensemble of seed-competent states that define M_s, each separated by smaller barriers. Using this multimodal model, we calculated the barrier to conversion of M_s to an inert form to be ~18 kcal / mol.

M_s has unique properties of self-assembly

Aggregation of M_i *in vitro* is relatively slow, requires high protein concentration (micromolar), and polyanions such as heparin(12,13). Based on the seeding activity of M_s we predicted that it might more readily self-associate. We incubated FL WT tau M_i and M_s alone, or dimer or trimer at equimolar ratios, keeping total particle concentration constant at 500nM. We then monitored change in assembly size over 24h. M_i, dimer, and trimer showed no evidence of self-association in this timeframe (Fig. 5A,C,D). By contrast, when incubated alone, M_s readily formed larger assemblies (Fig. 5B). When we incubated M_i with dimer or trimer, we saw no change in the assembly population over 24h (Fig. 5E,F). By contrast, when we mixed M_s with dimer or trimer we observed a growth of larger assemblies with a concomitant reduction in dimer and trimer peaks (Fig. 5G,H). We conclude that M_i, dimer, and trimer do not form larger assemblies at an appreciable rate, while M_s self-assembles or adds on to larger assemblies.

AD brain contains seed-competent monomer

Given our experiments with M_i and M_s, we wished to test whether similar structures exist *in vivo*, and thus isolated tau monomer from AD and control patient brains. We extracted brain samples using a dounce homogenizer gently to try to avoid liberating significant monomer from fibrils. We immunoprecipitated tau using an antibody that targets the amino-terminus, and resolved the eluates by SEC, followed by ELISA to determine tau levels (Fig. 6A,B). Whereas tau from control brain extract eluted in the monomer fraction (Fig. 6A), tau from AD brain distributed across multiple fractions, corresponding to monomer and larger assemblies (Fig. 6B). When we tested each fraction for seeding activity, we observed none in any control brain fraction, including monomer (Fig. 6C). However all AD fractions contained seeding activity, including monomer (Fig. 6C). A seed-competent tau monomer is thus present in AD brain, but not in control brain. To test for its self-association *in vitro*, we incubated control and AD monomer for up to 24h. We then resolved the assemblies via SEC and tested each fraction for seeding activity. At 0h, AD monomer exhibited seeding activity (Fig. 6D). Over time we observed a transition to larger seed-competent assemblies (Fig. 6E, F). Tau monomer derived from AD brain thus has an intrinsic capacity for self-association into seed-competent assemblies.

XL-MS reveals distinct, stable conformational states in recombinant tau monomer

To probe the structures of various forms of recombinant tau monomer, we employed crosslinking with mass spectrometry (XL-MS). This method creates restraints for structural models of single proteins or protein complexes(21,26,27). We studied FL WT tau monomer from a variety of conditions: recombinant protein purified from E. coli (M_r); the same protein exposed to heparin for 1min and purified by SEC (M_h); recombinant monomer subsequently

purified by SEC (M_i); and seed-competent monomer purified after sonication of fibrils (M_s). In each case, we performed reactions at low protein concentrations and short crosslink times, avoiding inter-protein crosslinks. We reacted samples with DSS, digested them with trypsin, enriched crosslinked peptides with by SEC, and analyzed them by capillary liquid chromatography tandem mass spectrometry. We assigned the complex fragment ion spectra to the corresponding peptide sequences using xQuest (22). Denaturation of recombinant tau with 8M urea prior to crosslinking produced no intramolecular cross-links (data not shown), indicating that crosslinks observed under native conditions represent local structure.

Given our observation that four forms of WT FL tau (M_r, M_h, M_i, M_s) had two distinct activities (inert vs. seed-competent), we compared their structures using XL-MS. M_r and M_h, despite different seeding activities, exhibited relatively similar intramolecular crosslink patterns. These were dominated by short-range crosslinks (Fig. 7A,B). In M_r, we identified 21 unique crosslinks evenly distributed within the repeat domain (RD: aa243-367, composed of four repeated ~30aa sequences, RD1-4), and the projection domain (PD: aa1-242), with an average sequence separation of 16.5 aa between modified lysines (Fig. 7A; S1A; Table S1). In M_h, 57 unique crosslinks had a similar average sequence separation of 16 aa between modified lysines (Fig. 7B; S1B; Table S1). We observed an increased abundance of short range crosslinks clustered into two main regions: PD (aa130-175), RD2 (aa270-290), and RD4 (aa350-400) (Fig. 7B, S7B and Table S1). M_i exhibited 7 crosslinks, and M_s exhibited 8 (Fig. 7C,D; S1C,D; Table S1). M_i and M_s shared only two common crosslinks, K224-K347 and K225-K347, and crosslinks differed within the RD and in regions just upstream and downstream (Fig. 7C,D). The average sequence separation for M_i was 113 aa, and for M_s it was 136 aa. We note differences between M_i (purified by SEC), and M_r (which was not). This may be due to residual cell components (e.g. RNA) bound to M_r. In summary, we observed mostly short-range crosslink patterns for M_r and M_h with different distributions in the RD. Importantly, the crosslink pattern of M_h was very different from that of M_s, indicating that heparin exposure alone does not account for the structure of M_s.

To test patient-derived tau monomer, we immunopurified tau from brains of 3 AD brains and 3 age-matched controls, using the established SEC protocol to purify seed-competent monomer followed by our XL-MS protocol. In control tau we observed 5-7 intramolecular crosslinks (Fig. 7E; Table S1) and in AD-derived tau we observed 10-13 intramolecular crosslinks (Fig. 7F; Table S1). Similar to recombinant M_s, in all AD tau monomer samples we observed a discrete set of crosslinks between aa150 and aa259-290 (Fig. 7E, red lines). To evaluate the variability in the preparation of the brain derived samples more precisely, we homogenized tissue from a single AD brain using different approaches ranging in severity: dounce homogenization, pulse sonication, mechanical homogenization, and mechanical homogenization with pulse sonication (Fig. S2A-D, Table S1). While there was variation in the total number of crosslinks (3, 11, 57, and 8, respectively) the core set of crosslinks between aa150 and 259-290 were present independent of homogenization method (Fig. S2A-D, red lines). The consistency of the crosslinks between aa150 and 259-290 focused our attention on the domains they implicated, especially the amyloid-forming sequences within the RD.

Models of seed-competent monomers suggest exposure of VQIINK and VQIVYK

To understand how core elements of tau might play a role in its aggregation, we employed ROSETTA to create models of tau structure for M_r, M_h, M_i and M_s, using restraints from the crosslink patterns, and length of the DSS crosslinker (Fig. 8A-D, Table S1, Supp. Movies: M_r,

M_h, M_i, M_s). We prioritized low energy structures that excluded additional contacts with the N- and C-termini, as suggested by the crosslink patterns (see methods for details). We next calculated protein contact maps for representative M_r and M_i (inert), and M_h, and M_s (seed competent) structures (Fig. S3A-D), which highlight how the XL-MS derived restraints drive the topology of each tau structure (Fig. S3E-H, green dots). The M_r structural model was based on short range contacts clustered throughout the entire RD (Fig. 8A), and this predicted masking of VQIINK and VQIVYK sequences, which have previously been proposed as critical for tau amyloid formation(28,29). The model of M_i structure was based on a dramatically different crosslink pattern, with the RD1/2 (Fig. 8C, red-green interface) and RD2/3 (Fig. 8C, green-blue interface) regions in discretely formed hairpins similar to the conformation of tau bound to microtubules indicated by NMR (30). In this model, the core elements of VQIINK (green spheres) at the beginning of the RD2, and VQIVYK (blue spheres) at the beginning of the RD3(29) are buried in hairpins (Fig. 8C, S3C). Remarkably, despite different crosslink patterns, our models suggested that both M_r and M_i feature VQIINK/VQIVYK sequences relatively obscured from solvent accessibility. Crosslink studies of tau monomer from control patients also suggested a structural model in which these core residues are less accessible (Fig. 8E, Table S1; Supp. Movie: Control 1), although we place important caveats on these interpretations. Our ability to resolve high confidence structural models using XL-MS in patient-derived samples is more limited due to fewer high confidence crosslinks, possibly from sample heterogeneity (multiple isoforms, and multiple tau structures).

For seed-competent forms of tau, and despite distinct crosslink patterns, we also observed common predicted effects on VQIINK/VQIVYK exposure. The M_h structural model was predominantly influenced by short-range crosslinks, consistent with local contacts within the PD and the RD2 that result in burial of the VQIINK sequence but exposure of the VQIVYK sequence (Fig. 8B; Supp. Movie: M_h). This is consistent with recent observations that heparin binds directly to residues 270-290 which include VQIINK (33). By contrast the model of M_s was influenced by more long-range crosslinks, which nonetheless predicted an exposed conformation of VQIINK/VQIVYK (Fig. 8D; Supp. Movie: M_s). Lastly, in AD brain-derived tau we also observed crosslinks between aa ~150 to aa259-290, which we think help define an exposed configuration of VQIINK/VQIVYK in a seed-competent monomer (Fig. 8F, Table S1; Supp. Movie: AD1). In summary, despite profound differences in overall crosslink patterns, the models suggested by XL-MS highlight relative exposure of VQIINK/VQIVYK in forms of tau with intrinsic seeding activity (M_h, M_s), while forms of tau that are inert (M_r, M_i) feature VQIINK/VQIVYK buried in hairpins. These models will obviously require additional tests using advanced biophysical methods, but provide a plausible explanation for the distinct activities of tau monomer that we have observed.

Discussion

The simplest interpretation of our data is that consistent with it being an intrinsically disordered protein, tau monomer can occupy several unique and stable conformational states. One set of structures is relatively inert, while another has intrinsic ability to self-assemble, and acts as a template, or seed, for fibril growth *in vitro* and in cells. We confirmed with multiple controls that M_s, derived from sonicated fibrils, was in fact a monomer and not a larger assembly, and that there was no detectable cross-contamination of larger species into the putative monomer fraction upon SEC. Heat denaturation of seeding activity was

consistent with a complex folding state for M_s, comprised of several seed-competent intermediates. Tau monomer purified from AD brain also had intrinsic seeding activity, and self-associated to produce seed-competent assemblies. Finally, we used XL-MS to compare conformations of different tau monomers. A model restrained by our XL-MS data suggested that VQIVYK and VQIINK sequences might assume an open configuration in M_s, M_h, and AD-derived monomer, all of which have intrinsic seeding activity. By contrast, the model suggested that M_i and M_r, and control brain monomer, all of which are inert, lack VQIINK/VQIVYK exposure. Taken together, these data establish a new concept for tau: this intrinsically disordered protein has multiple, stable monomeric states, functionally distinguished by the presence or absence of seeding activity.

Amyloid proteins form progressively larger assemblies over time, and it has been difficult to define the composition of the minimal seed. Mandelkow and colleagues studied tau aggregation *in vitro* and concluded that a seed of 8-12 molecules existed in their experimental system(3). By contrast, Kuret and colleagues posited an “intermediate” of tau that could subsequently initiate self-assembly, and their data, based on extrapolation of tau concentrations needed to enable development of thioflavin fluorescence *in vitro*, were consistent with a monomeric seed(1). Wetzel and colleagues also proposed that a monomer is the basis of a “thermodynamic nucleus” that templates the aggregation of synthetic polyglutamine peptides(31). However, no prior study has previously identified stable forms of tau that seed amyloid formation. This provides an opportunity to study the earliest events in aggregate formation.

The actual cause of tau aggregation in tauopathies is unknown. It has been proposed that dissociation of tau monomer from microtubules, possibly due to phosphorylation, allows self-association to form pathogenic assemblies(32). In this study, using a single source of recombinant protein, we define distinctly structured seed-competent and inert forms of tau. We have similarly identified seed-competent species in patient-derived preparations. We fully recognize that in reality “seed-competent” and “inert” forms of tau represent multiple structural ensembles separated by defined energy or kinetic barriers. The barrier blocking conversion of an inert to a seed-competent form of tau can apparently be overcome by incubation with heparin and/or incorporation into a fibril. In neurons, other factors such as post-translational modifications and heterologous binding events likely play a role. Identification of the factors that trigger conversion from inert to seed-competent forms will thus have obvious implications for understanding disease mechanisms.

Isolation of seed-competent monomer from AD brain, with a very mild purification that explicitly excludes sonication or vigorous tissue homogenization, strongly suggests that this form of monomer freely exists *in vivo*. Furthermore, we observed that both recombinant M_s and AD -derived monomer build multimeric assemblies *in vitro* far more efficiently than M_i or control-derived monomer. Thus we hypothesize that a uniquely structured form of tau may be required for efficient assembly growth in cells. This contrasts with the idea that multimeric assemblies uniquely stabilize the conformation of otherwise unstructured proteins as they incorporate into the growing fibril. Taken together, we imagine that the initiation of aggregation in human brain might begin with conversion of tau monomer from an inert to a seed-competent form. To fully study this process will require more extensive biochemical purification of tau monomer from the earliest stages of disease.

M_s has a remarkably stable structure, as it resists heat denaturation at 95°C for up to 3h. This suggests a heretofore unrecognized conformation of tau that, to account for its slow heat denaturation, likely involves multiple intra-molecular interactions involving short and long range amino acid contacts. XL-MS provides some indication of what these might be, and indicates a predominance of more long-range intramolecular interactions in M_s vs. M_i. In agreement with the XL-MS results, we observed that heat inactivation of M_s seeding activity occurs with a lag phase, rather than first order time-dependent decay. This is implies a complex tertiary structure in which M_s has multiple seed-competent intermediates. Future XL-MS studies performed at different temperatures could reveal these structures. With more advanced methods to interrogate the structure of monomeric tau in patient material, we imagine that "seed-competent monomer" will in fact represent myriad structures, depending on the underlying disease. This could provide an explanation for how a single protein might self-assemble into diverse amyloid strains.

Without further studies to identify structures of tau at higher resolution, we cannot know for certain why one form acts as a seed and the other does not. However, we gained important insights when we modeled tau structures using ROSETTA, using XL-MS results as restraints. Despite obvious caveats, our models predict that the local environment surrounding two hexapeptide motifs, VQIINK and VQIVYK, which are required for tau to form amyloid structures, may explain the differences between seed-competent and inert forms. In the models of M_i and M_r, and control brain-derived tau, these motifs lie buried in hairpin structures, whereas in M_s and AD-derived tau, both are exposed, and in M_h VQIVYK is exposed. VQIINK/VQIVYK thus might serve as substrates for intermolecular interaction in a growing assembly. Interestingly, M_s has a very different pattern of crosslinks compared to the M_h, yet both seed aggregation. Indeed, it has been recently observed that heparin binding involves residues spanning 270-290, and promotes expansion of the remainder of the molecule (33), which is consistent with our predictions of relative exposure of VQIINK/VQIVYK. We hypothesize that conformers of tau monomer differentially present the core VQIINK/VQIVYK sequences. The diversity of exposed core elements (potentially beyond VQIINK/VQIVYK) could specify the formation of assemblies that give rise to distinct strains. Consistent with this idea, a recent structural study indicates that in AD-derived tau fibrils the VQIVYK sequence plays a key role in the core amyloid structure along with adjacent amino acids, but the VQIINK sequence does not (34). We also note that multiple disease-associated mutations in tau affect residues in close proximity to VQIINK/VQIVYK. For example, our models predict that serine or leucine substitutions at P301 (which cause dominantly inherited tauopathy) would destabilize the local structure, and promote exposure of the VQIINK/VQIVYK sequences. Future experiments will test these ideas more definitively.

Conclusion

Our findings indicate that tau monomer has at least two dominant structural configurations, one of which has intrinsic activity as a seed and a self-assembly factor. We cannot exclude other models of seed formation based on these studies, and they may also play a key role in amyloid formation. Thus even temporary, critical local elevations in the concentration of an aggregation-prone protein may enable clustering, with an as yet unspecified conformational transition to form a seed. This would be consistent with a "molten globule" as the origin of a seed, perhaps reflecting the multimeric tau assembly described originally by Mandelkow and colleagues (3). However, our observations in this case suggest an alternative possibility, whereby events triggered by aging, genetics, beta amyloid toxicity, brain trauma, or other

insults, enable tau monomer to transition to a stable conformation that mediates self-assembly and initiates tauopathy.

Acknowledgements

We thank Peter Davies for generously providing antibody reagents and ELISA protocol guidance. This work was supported by grants from the Tau Consortium and NIH grants awarded to 1R01NS071835 (M.I.D.), R01NS089932 (R.V.P. and M.I.D.), and the Effie Marie Cain Endowed Scholarship (L.A.J.). We appreciate the help of the Live Cell Imaging Core Facility administered by Katherine Luby-Phelps, Ph.D., and the Proteomics Core Facility at the University of Texas Southwestern Medical Center.

Competing Interests

A patent disclosure has been filed by H.M., L.A.J. and M.I.D. related to the use of unique crosslinks to create biomarkers for neurodegenerative diseases.

References

1. Chirita CN, Congdon EE, Yin H, Kuret J. Triggers of full-length tau aggregation: a role for partially folded intermediates. Biochemistry. 2005 Apr 19;44(15):5862–72.

2. Kar K, Jayaraman M, Sahoo B, Kodali R, Wetzel R. Critical nucleus size for disease-related polyglutamine aggregation is repeat-length dependent. Nat. Struct. Mol. Biol. 2011 Mar;18(3):328–36. PMCID: PMC3075957

3. Friedhoff P, Bergen von M, Mandelkow EM, Davies P, Mandelkow E. A nucleated assembly mechanism of Alzheimer paired helical filaments. Proc. Natl. Acad. Sci. U.S.A. National Academy of Sciences; 1998 Dec 22;95(26):15712–7. PMCID: PMC28109

4. Neurodegenerative tauopathies. 2001;24(1):1121–59. Retrieved from: http://www.annualreviews.org/doi/abs/10.1146/annurev.neuro.24.1.1121

5. Sanders DW, Kaufman SK, Holmes BB, Diamond MI. Prions and Protein Assemblies that Convey Biological Information in Health and Disease. Neuron. Elsevier; 2016 Feb 3;89(3):433–48. PMCID: PMC4748384

6. Tau Trimers Are the Minimal Propagation Unit Spontaneously Internalized to Seed Intracellular Aggregation. 2015 Jun 12;290(24):14893–903. PMCID: PMC4463437

7. Frost B, Jacks RL, Diamond MI. Propagation of tau misfolding from the outside to the inside of a cell. J. Biol. Chem. American Society for Biochemistry and Molecular Biology; 2009 May 8;284(19):12845–52. PMCID: PMC2676015

8. Proteopathic tau seeding predicts tauopathy in vivo. 2014 Oct 14;111(41):E4376–85. PMCID: PMC4205609

9. Holmes BB, Devos SL, Kfoury N, Li M, Jacks R, Yanamandra K, et al. Heparan sulfate proteoglycans mediate internalization and propagation of specific proteopathic seeds. Proc. Natl. Acad. Sci. U.S.A. National Acad Sciences; 2013 Aug 13;110(33):E3138–47. PMCID: PMC3746848

10. Sanders DW, Kaufman SK, Devos SL, Sharma AM, Mirbaha H, Li A, et al. Distinct Tau Prion Strains Propagate in Cells and Mice and Define Different Tauopathies. Neuron. 2014 May 21. PMCID: PMC4171396

11. Furman JL, Holmes BB, Diamond MI. Sensitive Detection of Proteopathic Seeding Activity with FRET Flow Cytometry. J Vis Exp. 2015;(106):e53205–5. PMCID: PMC4692784

12. Goedert M, Jakes R, Spillantini MG, Hasegawa M, Smith MJ, Crowther RA. Assembly of microtubule-associated protein tau into Alzheimer-like filaments induced by sulphated glycosaminoglycans. Nature. Nature Publishing Group; 1996 Oct 10;383(6600):550–3.

13. Pérez M, Valpuesta JM, Medina M, Montejo de Garcini E, Avila J. Polymerization of tau into filaments in the presence of heparin: the minimal sequence required for tau-tau

768 interaction. J. Neurochem. 1996 Sep;67(3):1183–90.

769 14. Frost B, Ollesch J, Wille H, Diamond MI. Conformational diversity of wild-type Tau
770 fibrils specified by templated conformation change. J. Biol. Chem. American Society for
771 Biochemistry and Molecular Biology; 2009 Feb 6;284(6):3546–51. PMCID:
772 PMC2635036

773 15. Acker CM, Forest SK, Zinkowski R, Davies P, d'Abramo C. Sensitive quantitative
774 assays for tau and phospho-tau in transgenic mouse models. Neurobiol. Aging. 2013
775 Jan;34(1):338–50. PMCID: PMC3474864

776 16. Measurement of microsecond dynamic motion in the intestinal fatty acid binding protein
777 by using fluorescence correlation spectroscopy. 2002 Oct 29;99(22):14171–6.
778 Retrieved from:
779 http://eutils.ncbi.nlm.nih.gov/entrez/eutils/elink.fcgi?dbfrom=pubmed&id=12381795&ret
780 mode=ref&cmd=prlinks

781 17. Spectroscopic Study and Evaluation of Red-Absorbing Fluorescent Dyes. 2003
782 Jan;14(1):195–204. Retrieved from: http://pubs.acs.org/doi/abs/10.1021/bc025600x

783 18. Morozova OA, March ZM, Robinson AS, Colby DW. Conformational features of tau
784 fibrils from Alzheimer's disease brain are faithfully propagated by unmodified
785 recombinant protein. Biochemistry. American Chemical Society; 2013 Oct
786 8;52(40):6960–7. PMCID: PMC4142060

787 19. Laidler KJ. The development of the Arrhenius equation. Journal of Chemical Education.
788 1984.

789 20. Burnham KP, Anderson DR. Model selection and multimodal inference: a practical
790 information-theoretic approach. p. 61–3.

791 21. Leitner A, Joachimiak LA, Bracher A, Mönkemeyer L, Walzthoeni T, Chen B, et al. The
792 Molecular Architecture of the Eukaryotic Chaperonin TRiC/CCT. Structure. 2012
793 May;20(5):814–25.

794 22. Rinner O, Seebacher J, Walzthoeni T, Mueller LN, Beck M, Schmidt A, et al.
795 Identification of cross-linked peptides from large sequence databases. Nat. Methods.
796 Nature Publishing Group; 2008 Apr;5(4):315–8. PMCID: PMC2719781

797 23. Grimm M, Zimniak T, Kahraman A. xVis: a web server for the schematic visualization
798 and interpretation of crosslink-derived spatial restraints. Nucleic acids …. 2015.

799 24. Kahraman A, Herzog F, Leitner A, Rosenberger G, Aebersold R, Malmström L. Cross-
800 link guided molecular modeling with ROSETTA. Fernandez-Fuentes N, editor. PLoS
801 ONE. Public Library of Science; 2013;8(9):e73411. PMCID: PMC3775805

802 25. Lange OF, Rossi P, Sgourakis NG. Determination of solution structures of proteins up
803 to 40 kDa using CS-Rosetta with sparse NMR data from deuterated samples. 2012.

804 26. Lasker K, Förster F, Bohn S, Walzthoeni T, Villa E, Unverdorben P, et al. Molecular

architecture of the 26S proteasome holocomplex determined by an integrative approach. Proc. Natl. Acad. Sci. U.S.A. National Acad Sciences; 2012 Jan 31;109(5):1380–7. PMCID: PMC3277140

27. Joachimiak LA, Walzthoeni T, Liu CW, Aebersold R, Frydman J. The structural basis of substrate recognition by the eukaryotic chaperonin TRiC/CCT. Cell. 2014 Nov 20;159(5):1042–55. PMCID: PMC4298165

28. Bergen von M, Friedhoff P, Biernat J, Heberle J, Mandelkow EM, Mandelkow E. Assembly of tau protein into Alzheimer paired helical filaments depends on a local sequence motif ((306)VQIVYK(311)) forming beta structure. Proc. Natl. Acad. Sci. U.S.A. National Academy of Sciences; 2000 May 9;97(10):5129–34. PMCID: PMC25793

29. Bergen von M, Barghorn S, Li L, Marx A, Biernat J, Mandelkow EM, et al. Mutations of tau protein in frontotemporal dementia promote aggregation of paired helical filaments by enhancing local beta-structure. J. Biol. Chem. 2001 Dec 21;276(51):48165–74.

30. Kadavath H, Jaremko M, Jaremko Ł, Biernat J, Mandelkow E, Zweckstetter M. Folding of the Tau Protein on Microtubules. Angew. Chem. Int. Ed. Engl. WILEY-VCH Verlag; 2015 Aug 24;54(35):10347–51.

31. Bhattacharyya AM, Thakur AK, Wetzel R. polyglutamine aggregation nucleation: thermodynamics of a highly unfavorable protein folding reaction. Proc. Natl. Acad. Sci. U.S.A. 2005 Oct 25;102(43):15400–5. PMCID: PMC1266079

32. Mandelkow E-M, Mandelkow E. Biochemistry and cell biology of tau protein in neurofibrillary degeneration. Cold Spring Harb Perspect Med. 2012 Jul;2(7):a006247–7. PMCID: PMC3385935

33. Zhao J, Huvent I, Lippens G, Eliezer D, Zhang A, Li Q, et al. Glycan Determinants of Heparin-Tau Interaction. Biophys. J. 2017 Mar 14;112(5):921–32. PMCID: PMC5355497

34. Fitzpatrick AWP, Falcon B, He S, Murzin AG, Murshudov G, Garringer HJ, et al. Cryo-EM structures of tau filaments from Alzheimer's disease. Nature. 2017 Jul 5;56:343.

FIGURE LEGENDS

Figure 1: Isolation of recombinant tau assemblies and seeding activity of monomer derived from fibrils in cells and in vitro. (**A, B**) FL Cys-Tau(2A) was labeled with Alexa488 and resolved by SEC (A), or was fibrillized in the presence of heparin, labeled with Alexa488, sonicated, and the assemblies resolved by SEC (B). The column was calibrated using MW standards of the indicated sizes. Color codes indicate the putative assembly sizes. (**C**) Tau assemblies purified by SEC were evaluated by seeding onto tau RD-CFP/YFP biosensor cells. M_i represents "inert" monomer purified by SEC without fibrillization, which has no seeding activity; M_s represents "seed-competent" monomer purified after prior fibrillization and sonication. (**D**) FL WT tau and FL Cys-Tau(2A) were similarly fibrillized, sonicated, and the fragments resolved by SEC. Seeding activity of each fraction was evaluated by SEC. M_s and larger assemblies of both forms of tau exhibit seeding activity, but not M_i. Fractions were evaluated by FCS. IFD = Integrated FRET Density. (**E**) Heparin treatment of FL WT tau was carried out for 15min, 1h, or 4h. Samples were resolved by SEC, and fractions of various sizes were compared using the biosensor seeding assay. "Pre-SEC" refers to the sample prior to fractionation. At 15min, a small, but significant seeding activity was observed in the monomer fraction. By 1h this was very strong, and was comparable to the signal from monomer derived from sonicated fibrils. NT = monomer not treated with heparin. (**F**) Full-length (0N4R) tau aggregation *in vitro* was measured using induced thioflavin fluorescence. Fibril-derived samples were purified by SEC. M_i had no seeding activity, whereas M_s, trimer, and unfractionated fibrils had strong seeding activity.

Figure 2: Fluorescence correlation spectroscopy (FCS) analyses of M_i and M_s. (**A**) CD spectra of M_i and M_s were similar. (**B**) FCS Diffusion times for M_i, M_S, dimer, trimer, and ~10mer, and the cross-correlation for M_i, M_s, dimer, trimer, and ≥10-mer were determined after labeling of fibrils with Alexa488, or double labeling with tetramethylrhodamine prior to sonication. Table reflects the predicted diffusion time based on a molecular weight, and the actual diffusion time. The variance between predicted vs. observed times is reported. (**C-G**) FCS for double-labeled tau assemblies. Cross correlation between the two dyes is indicated in grey lines. (**H**) Summary of FCS cross-correlation, including free dyes. Neither free dye, M_i nor M_s showed any cross-correlation, indicating single species predominate. All multimeric assemblies exhibited cross-correlation, indicating the presence of both dyes within a single particle.

Figure 3: Seeding potency, SEC purification fidelity, and heat stability. (**A,B**) Titration of assemblies was performed. (A) M_s exhibited an EC_{50} of approximately 10nM (monomer equivalent); (B) Dimer and trimer had similar potencies. Concentration is reflected as monomer equivalent. (**C**) SEC fidelity was tested by isolating M_s from fractions after fibril sonication. Remaining fractions were combined with M_i, and the mix was re-isolated by SEC. (**D**) In Group 1, after the first isolation, the monomer fraction (which contains M_s) contained seeding activity. (**E**) In Group 2, after the second purification by SEC, the monomer fraction (which contains M_i spiked in) did not exhibit seeding activity. (**F-H**) Heat-induced dissociation of assemblies. (F) The SEC fraction containing M_s (B5) was heated to 95°C for 3h and re-isolated by SEC prior to testing the FRET biosensor assay. No loss in seeding activity was observed. (G) When the SEC fraction containing trimer (B8) was heated similarly, seeding activity shifted to fractions that contain dimer and monomer (B7, B5). (H) ~20-mer (A5) was largely stable to heating, although some smaller seed-competent assemblies were liberated.

Figure 4: Heat denaturation of assemblies. (**A-D**) Various assemblies were subjected to heat denaturation at the indicated temperatures and times, followed by analysis of seeding activity in the FRET biosensor assay. Whereas ~10-mer and ~20-mer were relatively stable from 65-95°C, monomer, dimer and trimer showed temperature-dependent loss of seeding activity. (**E**) Plot of denaturation data with multimodel regression curves superimposed.

Figure 5: M_s uniquely self-assembles. M_i and M_s were incubated at 500nM or with equivalent amounts (monomer equivalent) of dimer and trimer for various times prior to resolution by SEC. (**A**) M_i alone shows no capacity for self-association. (**B**) M_s exhibits self-association over time. (**C,D**) Dimer and Trimer are stable when incubated over time. (**E,F**) M_s reacts with dimer and trimer to form larger assemblies. (**G,H**) M_i does not react with dimer or trimer to form larger assemblies.

Figure 6: AD brain contains seed-competent monomer. Tau from AD and control brains was immunoprecipitated and subjected to SEC. (**A**) SEC from control brain shows predominantly tau monomer. (**B**) SEC from AD brain shows a range of tau assembly sizes. (**C**) Monomer from AD brain has seeding activity, but not monomer from control brain. Tau Unit refers to the putative number of molecules per assembly; C = Lipofectamine control. (**D,E**) Control or AD tau monomer was incubated for 0 (graph D) or 24h (graph E) prior to SEC, and seeding activity was determined from each fraction. Pre-SEC samples are shown at the first data point. After 24h incubation, AD-derived tau monomer exhibited seeding activity in fractions consistent with larger assemblies. (**F**) AD-derived tau monomer was incubated for the indicated times prior to SEC and determination of seeding activity in each fraction. Larger seed-competent assemblies formed in a time-dependent fashion.

Figure 7. Unique XL-MS patterns for different forms of tau monomer. Tau monomer was prepared as described and subjected to chemical crosslinking, digestion, and mass spectrometry to define intramolecular crosslinks. Cartoons represent crosslinks within the tau protein. Tau is shown in grey; RD is colored in red (R1), green (R2), blue (R3) and indigo (R4). High confidence XL-MS crosslinks are shown as light yellow lines; crosslinks consistent between the M_s and AD monomer are shown in red. (**A**) M_r: tau monomer prior to SEC. (**B**) M_h: tau monomer exposed to heparin, isolated by SEC; (**C**) M_i: tau monomer isolated by SEC; (**D**) M_s: tau monomer from fragmented fibrils, isolated by SEC. (**E**) AD brains contain long-range intramolecular crosslinks very similar to those observed in M_s (from 150 to 259-290). (**F**) Tau monomer from controls lacks the long range contacts observed in monomer from AD.

Figure 8. Models of different tau structures.
XL-MS results were used as restraints in Rosetta to create selected structural models of (**A**) M_r , (**B**) M_h , (**C**) M_i, (**D**) M_s, (**E**) Control monomer and (**F**) AD monomer. Tau protein sequence is shown in ribbon with the RD colored as in Figure 7. Regions between RD1/2 and RD2/3 are expanded, highlighting the two amyloid forming regions, VQIINK (green spheres) and VQIVYK (blue spheres). Note that in M_h, M_s and AD monomer the VQIINK and VQIVYK sequences are presented at the protein surface. In contrast, these regions are buried in M_r, M_i and control monomer. Please see Supplemental Movie files to better visualize the 3D orientation of specific regions.

Figure S1. XL-MS reveals differences in intramolecular crosslink distances between forms of tau monomer. Contact plots for XL-MS data for (**A**) M_r; (**B**) M_h; (**C**) M_i; (**D**) M_s

reveal different crosslink distances. The sites of XL-MS pairs are shown as green dots. Magenta boxes highlight differences in crosslink distance between the tau conformers. RD = repeat domain. PD = projection domain.

Figure S2. Different brain homogenization methods yield similar crosslink patterns. AD brain sample was homogenized using four different treatments (**A**) Dounce homogenization, (**B**) Pulse sonication, (**C**) Mechanical homogenization and (**D**) Mechanical homogenization followed by pulse sonication. Cartoons represent crosslinks within the tau protein. Tau is shown in grey; RD is colored in red (R1), green (R2), blue (R3) and indigo (R4). High confidence XL-MS crosslinks are shown as light yellow lines; crosslinks consistent with the M_s and AD monomers are shown in red.

Figure S3. Crosslinks maps in models reveal local structure. Models from Figure 8 protein contact map tau monomer structures reveal differences in crosslink distances in the repeat domain. (**A-D**) Models of tau monomer structure with crosslinks (yellow lines) superimposed. (**E-F**) Plot of crosslink distance colored according the atom pair distance in angstroms (Å) with a gradient from blue-red-yellow). The sites of XL-MS pairs are shown as green dots.

Table S1. Summary of XLMS datasets.

Supplemental Movie Files. PyMol was used to create rotating movies of all structural models for recombinant forms of tau (M_r, M_h, M_i and M_s) and monomer derived from Control 1 and AD 1 patient brains. We note that the model predicts that seed-competent forms of tau (M_h, M_s, AD) feature one or both VQIINK/VQIVYK sequences exposed. Inert forms of tau M_r, M_i, Control) feature these sequences relatively buried in hairpin structures. In tau derived from Control 1, the model predicts that VQIINK and VQIVYK sequences interact with one another within the monomer.

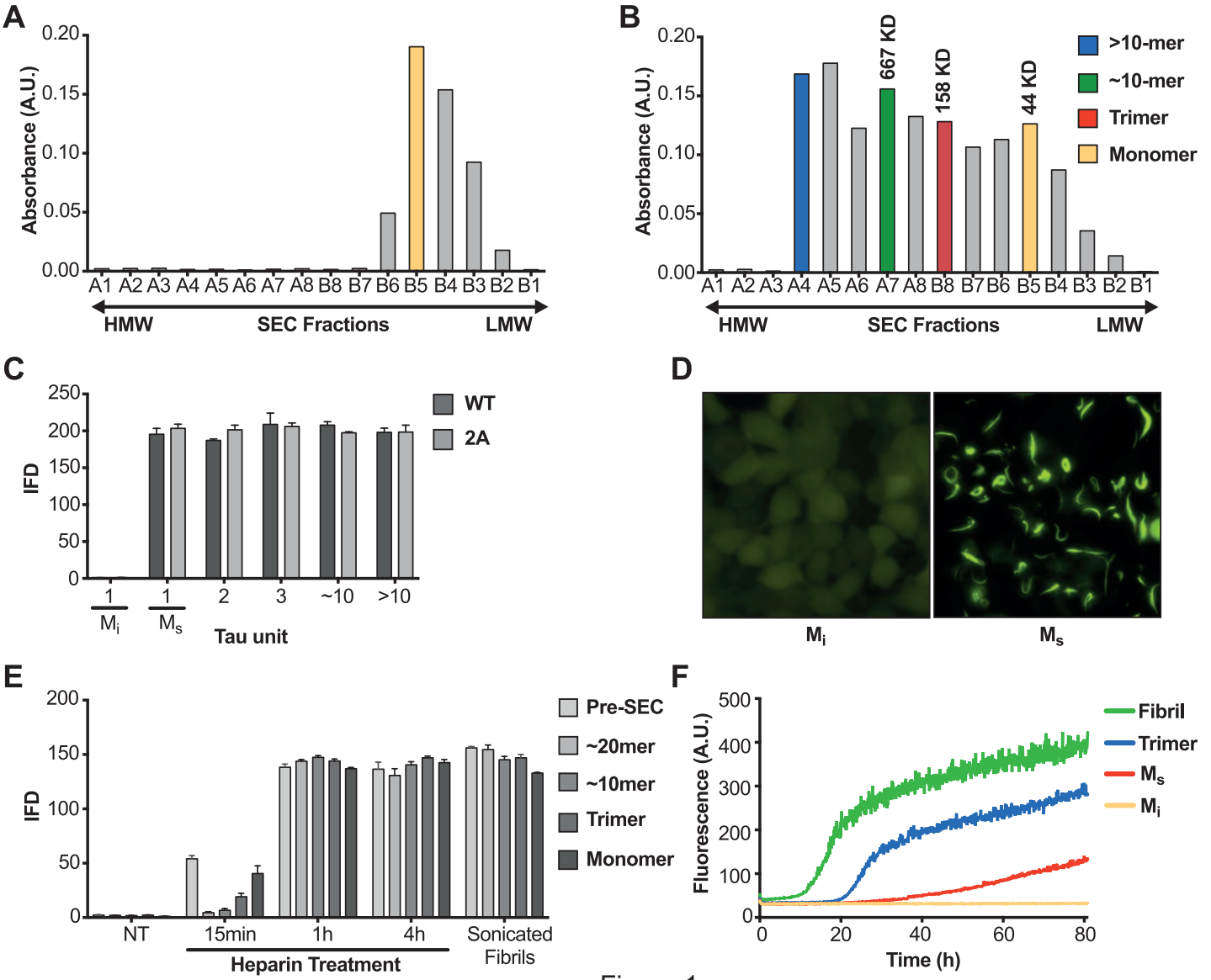
A
Absorbance (A.U.)
0.20
0.15
0.10
0.05
0.00
A1 A2 A3 A4 A5 A6 A7 A8 B8 B7 B6 B5 B4 B3 B2 B1
HMW
SEC Fractions
LMW
B
667 KD
158 KD
44 KD
>10-mer
~10-mer
Trimer
Monomer
C
IFD
250
200
150
100
50
0
WT
2A
1 1 2 3 ~10 >10
Mi Ms
Tau unit
D
Mi
Ms
E
IFD
200
150
100
50
0
Pre-SEC
~20mer
~10mer
Trimer
Monomer
NT
15min
1h
4h
Heparin Treatment
Sonicated Fibrils
F
Fluorescence (A.U.)
500
400
300
200
100
0
0 20 40 60 80
Time (h)
Fibril
Trimer
Ms
Mi

Figure 1

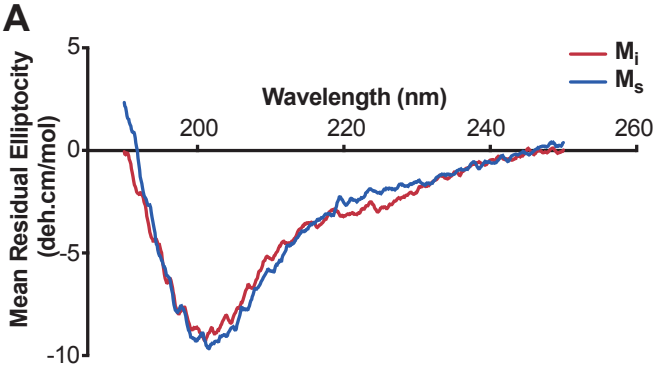

B

Fraction	Size (KD)	Units (n)	$T_{predicted}$ (µs)	T_{actual} (µs)	Variance*
B5	46	1	210	211	0.005
B7	92	2	264	270	0.022
B8	138	3	303	309	0.020
A7	667	10	452	561	0.241
A4	>667	>10	518	1880	0.724

*Variance: 1-(Predicted Diffusion Time/ Actual Diffusion Time)

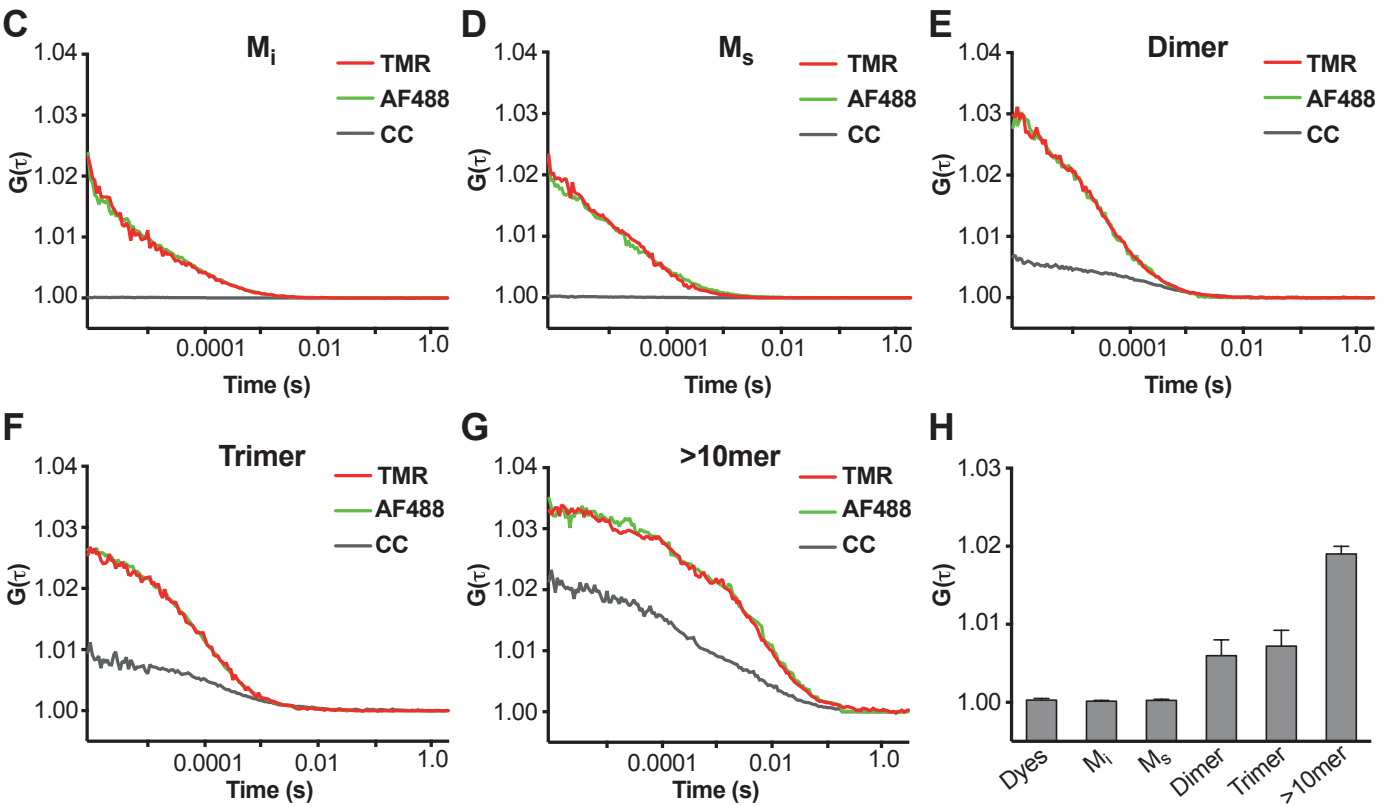

Figure 2

Figure 3

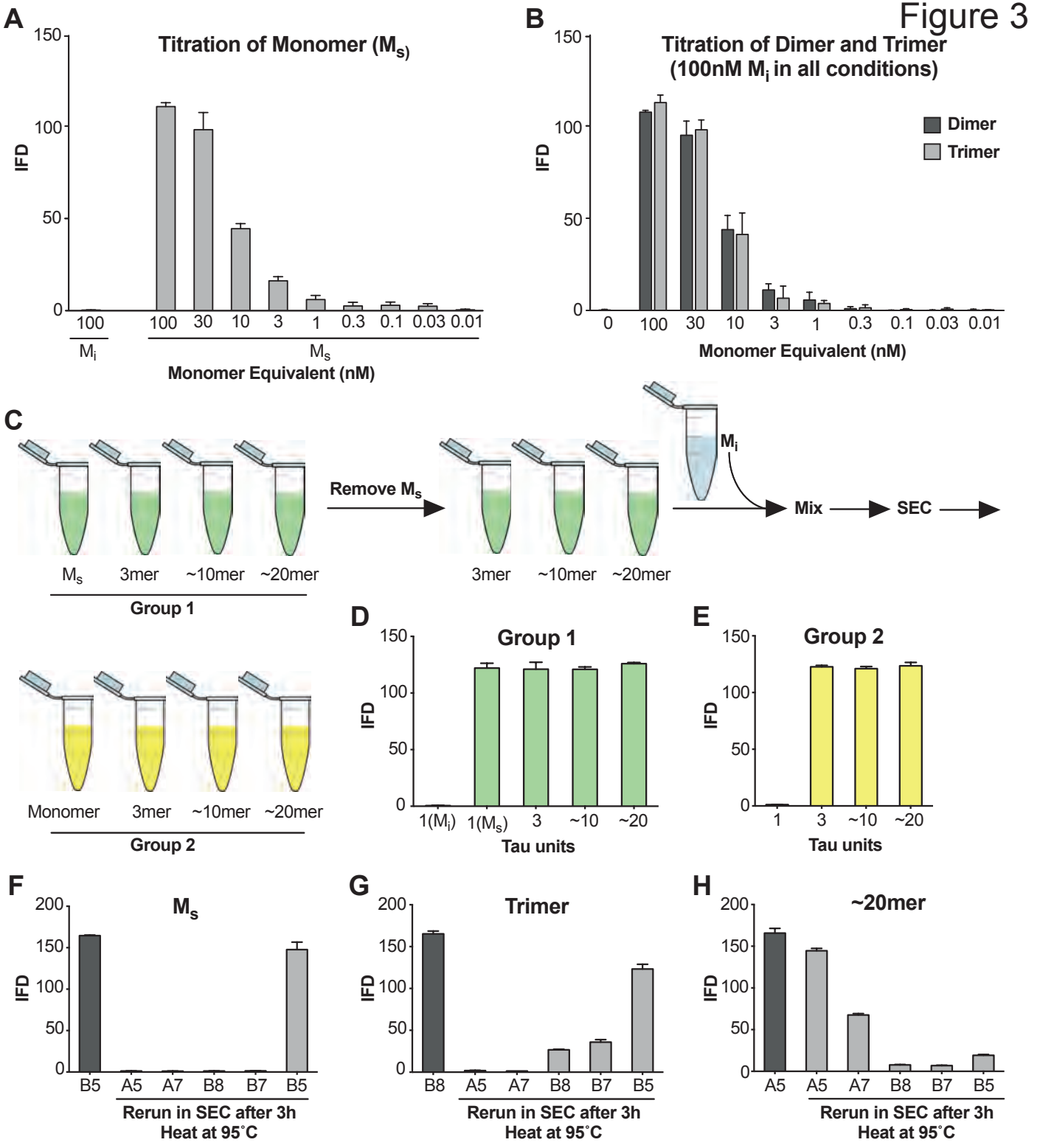
A
Titration of Monomer (M_s)
IFD
150
100
50
0
100
100 30 10 3 1 0.3 0.1 0.03 0.01
M_i
M_s
Monomer Equivalent (nM)
B
Titration of Dimer and Trimer
(100nM M_i in all conditions)
Dimer
Trimer
IFD
0 100 30 10 3 1 0.3 0.1 0.03 0.01
Monomer Equivalent (nM)
C
Remove M_s
M_i
Mix
SEC
M_s 3mer ~10mer ~20mer
Group 1
3mer ~10mer ~20mer
Monomer 3mer ~10mer ~20mer
Group 2
D
Group 1
IFD
1(M_i) 1(M_s) 3 ~10 ~20
Tau units
E
Group 2
IFD
1 3 ~10 ~20
Tau units
F
M_s
IFD
B5 A5 A7 B8 B7 B5
Rerun in SEC after 3h
Heat at 95˚C
G
Trimer
IFD
B8 A5 A7 B8 B7 B5
Rerun in SEC after 3h
Heat at 95˚C
H
~20mer
IFD
A5 A5 A7 B8 B7 B5
Rerun in SEC after 3h
Heat at 95˚C

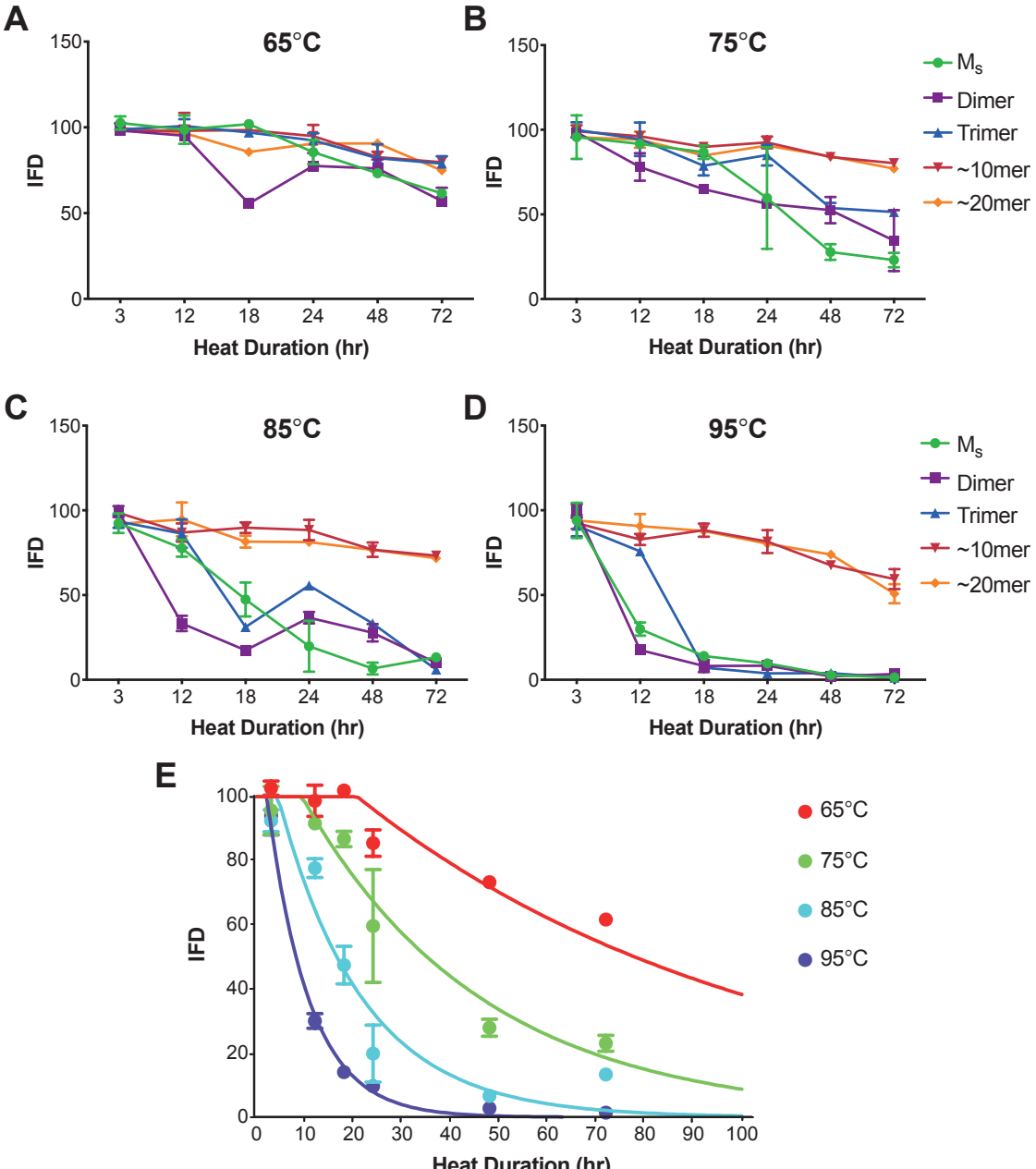
A
65°C
IFD
Heat Duration (hr)
B
75°C
C
85°C
D
95°C
Ms
Dimer
Trimer
~10mer
~20mer
E
65°C
75°C
85°C
95°C

Figure 4

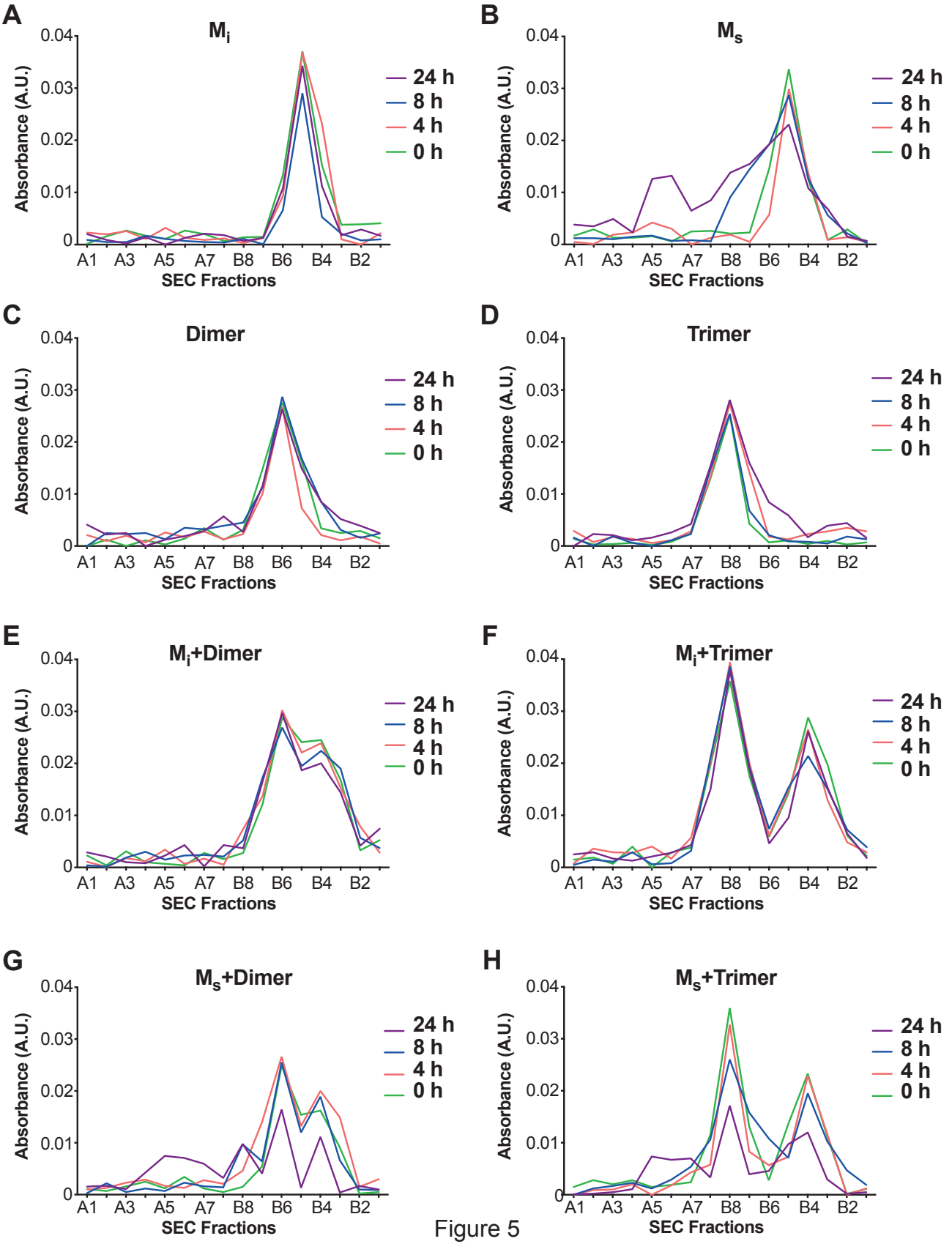
A
M_i
B
M_s
C
Dimer
D
Trimer
E
M_i+Dimer
F
M_i+Trimer
G
M_s+Dimer
H
M_s+Trimer
Absorbance (A.U.)
0.04
0.03
0.02
0.01
0
A1 A3 A5 A7 B8 B6 B4 B2
SEC Fractions
24 h
8 h
4 h
0 h

Figure 5

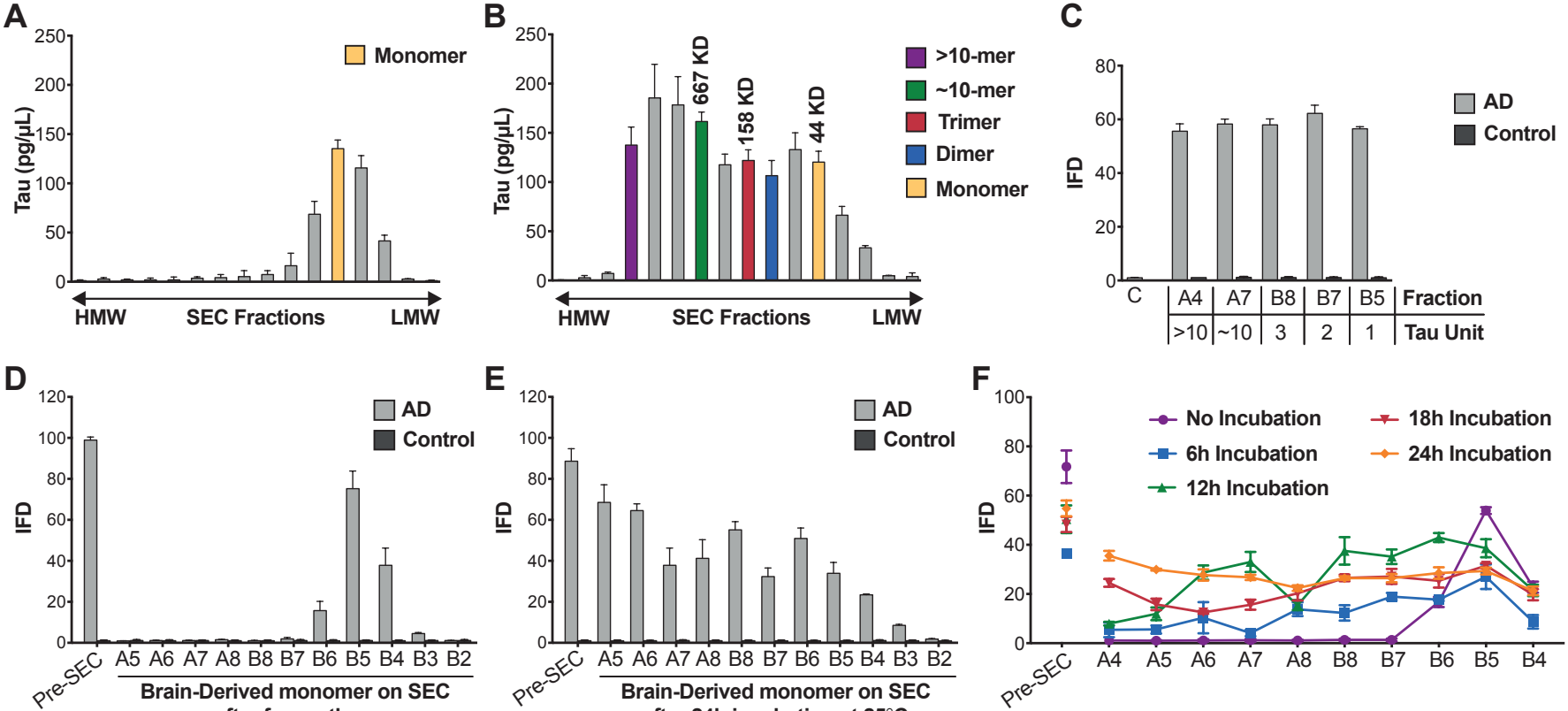
A
Tau (pg/μL)
Monomer
HMW
SEC Fractions
LMW
B
Tau (pg/μL)
667 KD
158 KD
44 KD
>10-mer
~10-mer
Trimer
Dimer
Monomer
HMW
SEC Fractions
LMW
C
IFD
AD
Control
C
A4
A7
B8
B7
B5
Fraction
>10
~10
3
2
1
Tau Unit
D
IFD
AD
Control
Pre-SEC
A5 A6 A7 A8 B8 B7 B6 B5 B4 B3 B2
Brain-Derived monomer on SEC
after freeze-thaw
E
IFD
AD
Control
Pre-SEC
A5 A6 A7 A8 B8 B7 B6 B5 B4 B3 B2
Brain-Derived monomer on SEC
after 24h incubation at 25°C
F
IFD
No Incubation
6h Incubation
12h Incubation
18h Incubation
24h Incubation
Pre-SEC
A4 A5 A6 A7 A8 B8 B7 B6 B5 B4

Figure 6

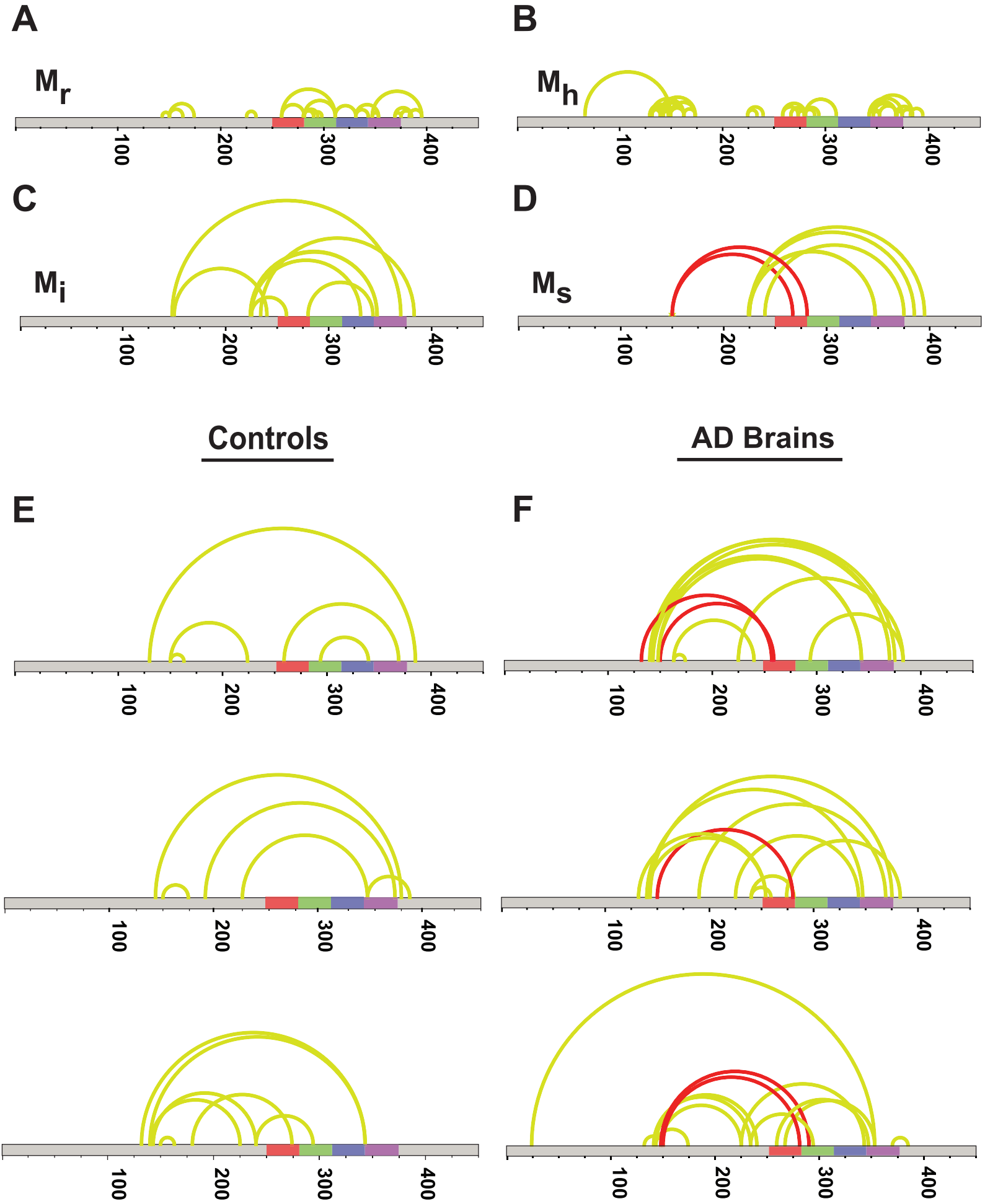

Figure 7

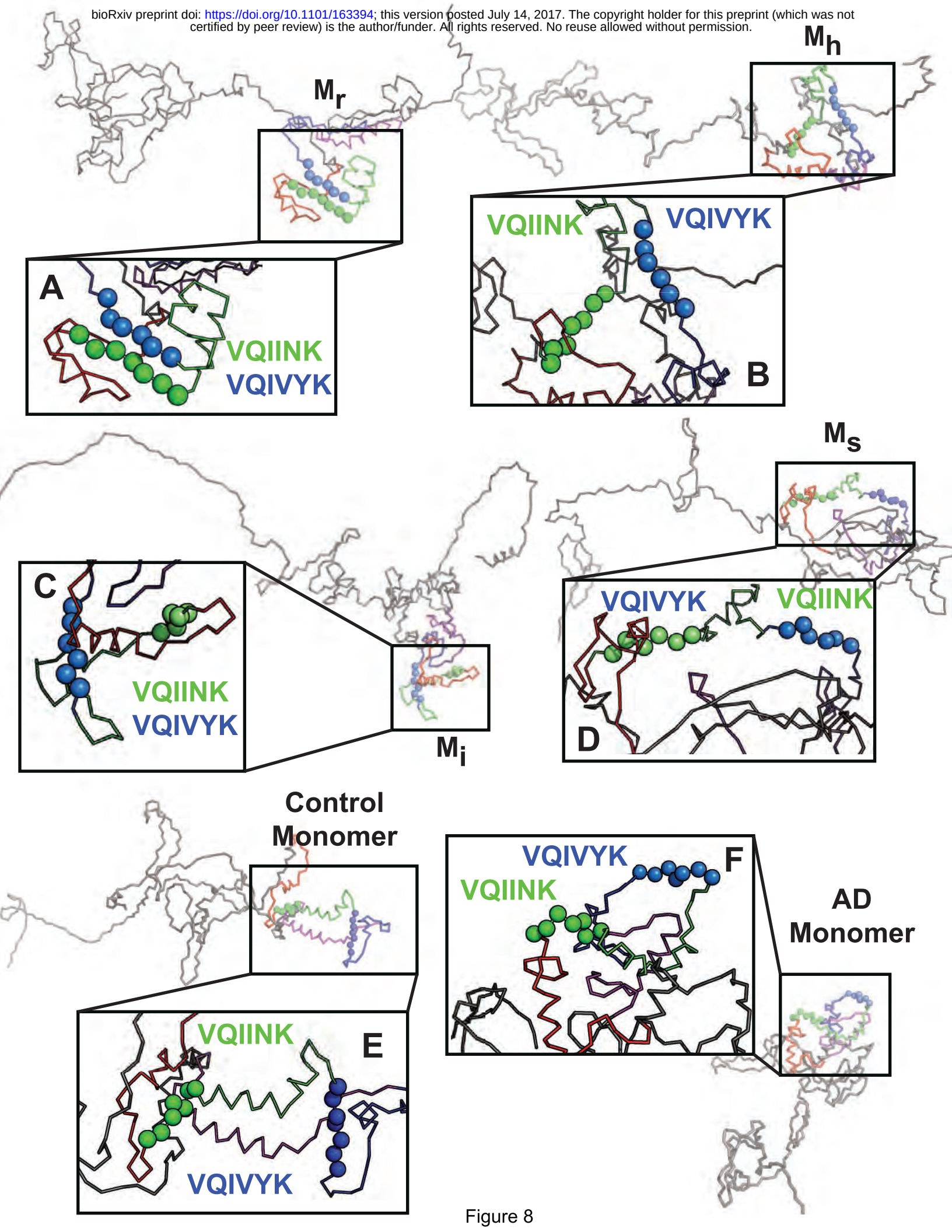

Figure 8

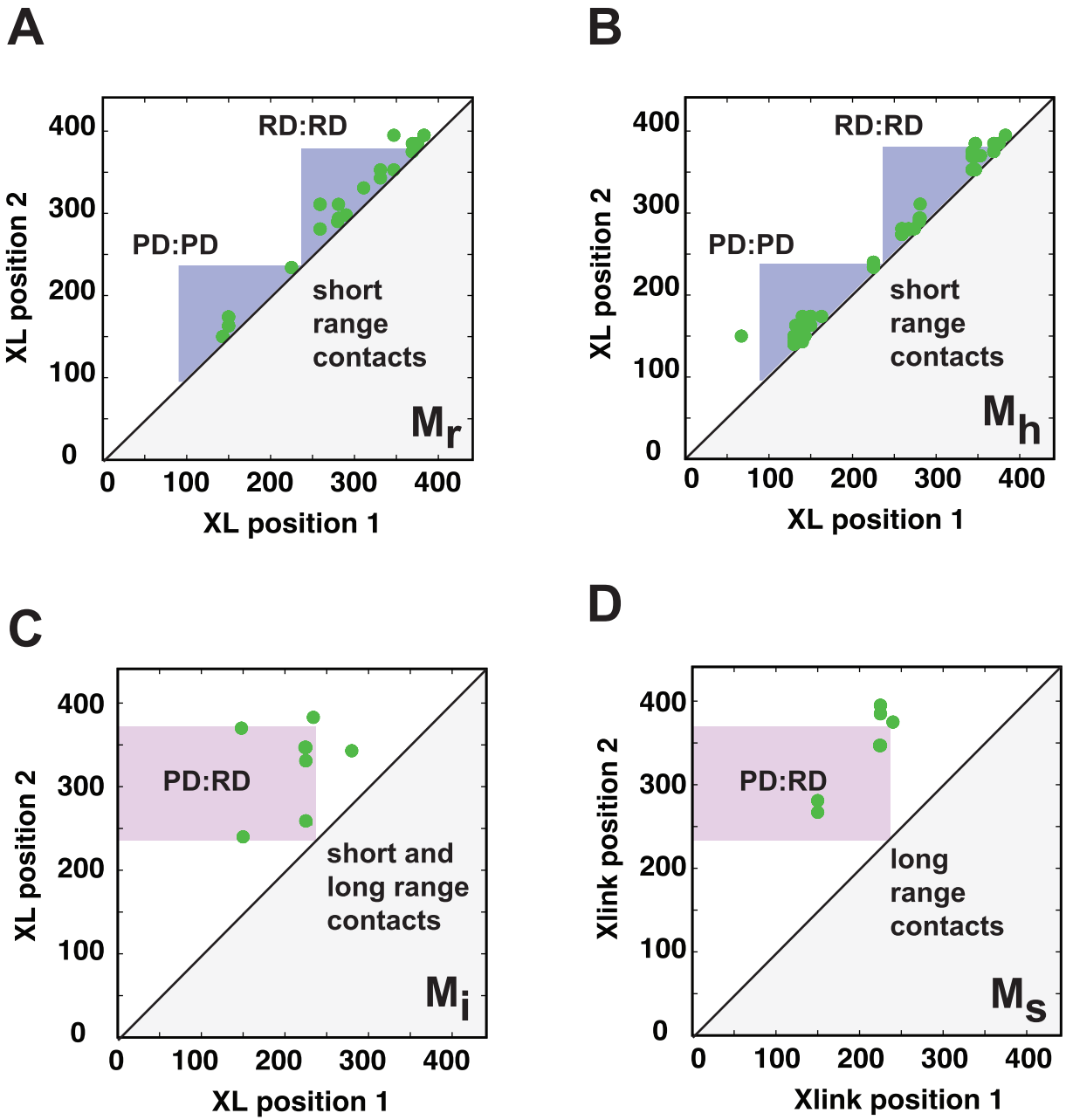

Supplemental Figure 1

A

Dounce Homogenization

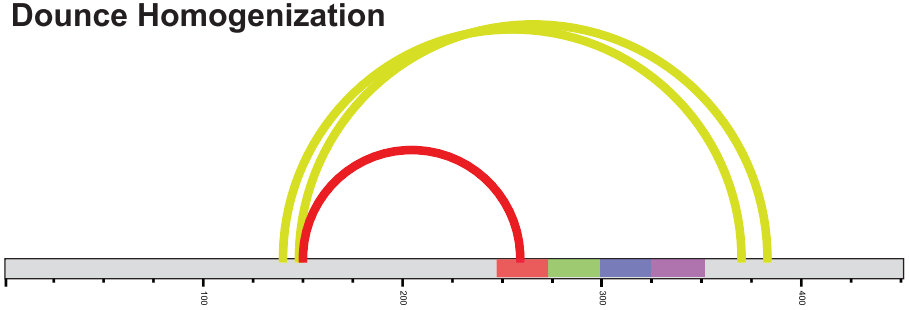

C

Mechanical Homogenization

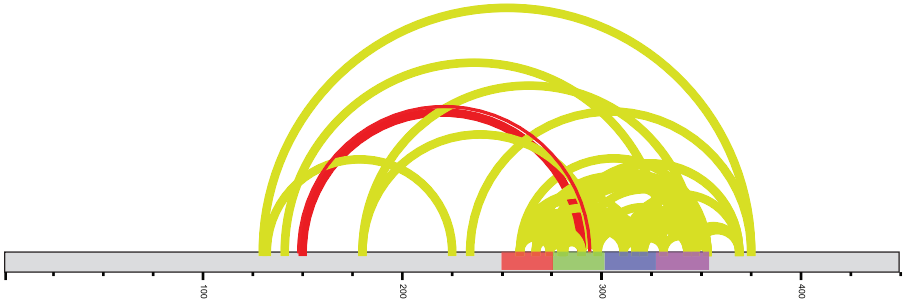

B

Pulse Sonication

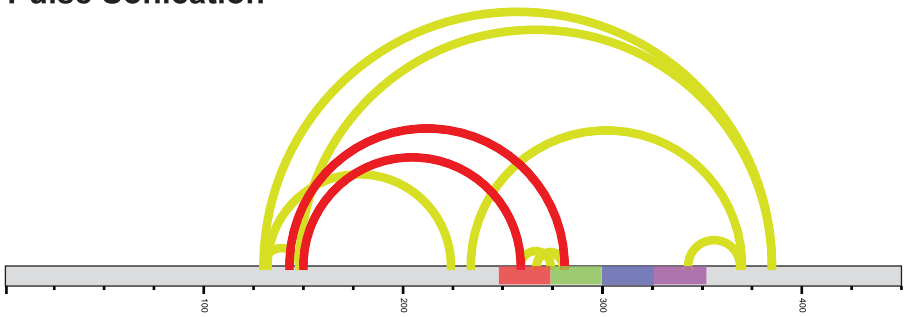

D

Mechanical Homogenization
Pulse Sonication

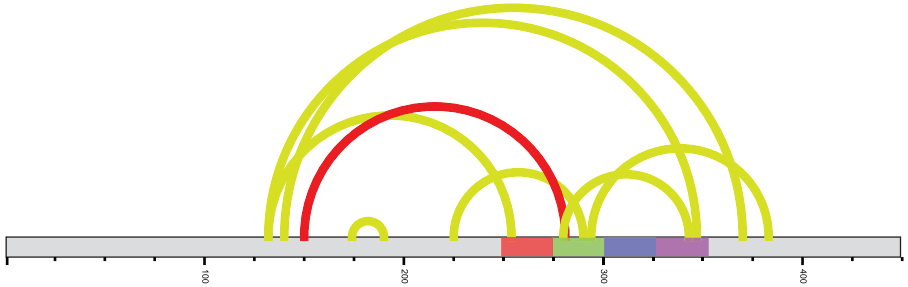

Supplemental Figure 2

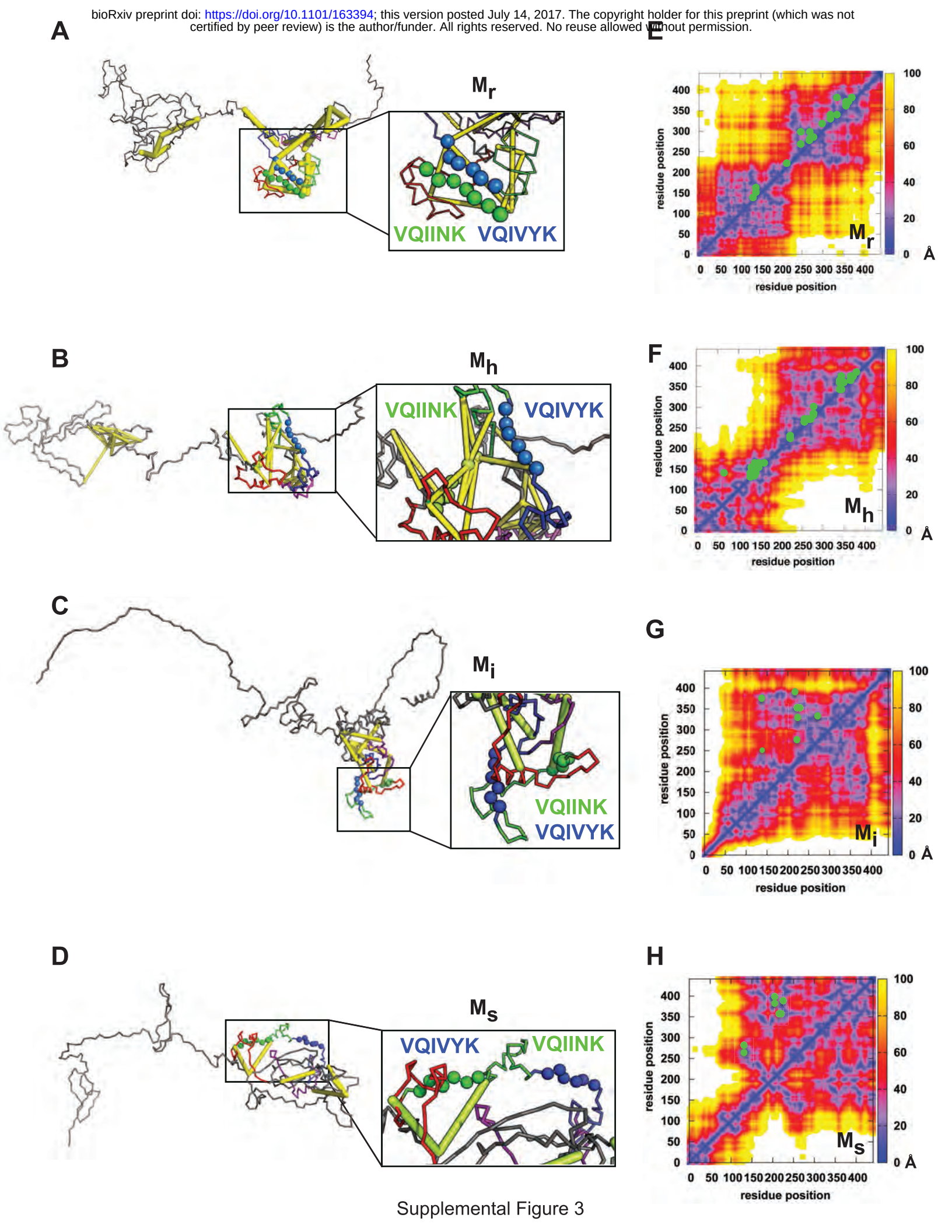

Supplemental Figure 3

Description of Column Headers

Id	Assigned peptides and cross-linking sites within the *peptide* sequences. The longer peptide is designated as (a)lpha, the shorter as (b)eta. Multiple positions are given in case of ambiguous assignments.
Protein1	SwissProt/UniProt accession number and identifier of the protein 1 (containing peptide desginated as alpha).
Protein1	SwissProt/UniProt accession number and identifier of the protein 2 (containing peptide desginated as beta).
XL Type	Type of cross-linked peptide
AbsPos1	Position in the protein sequence of protein 1, multiple positions are given in case of ambiguous assignments.
AbsPos2	Position in the protein sequence of protein 2, multiple positions are given in case of ambiguous assignments.
deltaAA	Delta between the absolute positions of the cross-linked residues
Mr	Molecular mass calculated from experimental m/z and z (neutral mass).
Mz	Experimentally observed mass-to-charge ratio of the precursor ion in Da.
z	Experimentally observed precursor charge.
Error [ppm]	Deviation between experimental and theoretical mass in ppm.
Id-score	Identification score as assigned by xQuest.

Mi XL-MS Data

Id	Protein1	Protein2	Type	XLType	AbsPos1	AbsPos2	deltaAA	Mr	Mz	z	Error_rel[ppm]	Id-Score
EPKKVAVVR-LDFKDR-a4-b4	TAU_HUMAN P10636-8	TAU_HUMAN P10636-8	xlink	intra-protein xl	225	347	122	1955.113	652.712	3	-3.8	12.57
TPSLPTPPTREPKK-SEKLDFKDR-a13-b7	TAU_HUMAN P10636-8	TAU_HUMAN P10636-8	xlink	intra-protein xl	224	347	123	2822.511	941.845	3	-2.4	11.97
VTSKCGSLGNIHHKPGGGQVEVKSEK-KVAVVR-a14-b1	TAU_HUMAN P10636-8	TAU_HUMAN P10636-8	xlink	intra-protein xl	331	225	106	3540.91	886.235	4	-2.7	11.61
SEKLDFKDR-VQIINKK-a3-b6	TAU_HUMAN P10636-8	TAU_HUMAN P10636-8	xlink	intra-protein xl	343	280	63	2116.186	706.403	3	-1.7	11.27
AKGADGKTK-KIETHK-a7-b1	TAU_HUMAN P10636-8	TAU_HUMAN P10636-8	xlink	intra-protein xl	148	370	222	1766.99	590.004	3	0.5	11.23
VAVVRTPPKSPSSAK-LTFRENAKAK-a9-b8	TAU_HUMAN P10636-8	TAU_HUMAN P10636-8	xlink	intra-protein xl	234	383	149	2837.603	710.409	4	-3.4	10.92
TPPKSPSSAKSR-TKIATPR-a10-b2	TAU_HUMAN P10636-8	TAU_HUMAN P10636-8	xlink	intra-protein xl	240	150	90	2165.223	722.749	3	2.9	10.39
SKIGSTENLK-EPKKVAVVR-a2-b4	TAU_HUMAN P10636-8	TAU_HUMAN P10636-8	xlink	intra-protein xl	259	225	34	2238.284	747.103	3	-4.6	10.26

Ms XL-MS Data

Id	Protein1	Protein2	Type	XLType	AbsPos1	AbsPos2	deltaAA	Mr	Mz	z	Error_rel[ppm]	Id-Score
IGSTENLKHQPGGGKVQIINK-GADGKTKIATPR-a8-b7	TAU_HUMAN P10636-8	TAU_HUMAN P10636-8	xlink	ntra-protein ›	267	150	117	3568.968	1190.664	3	-0.4	18.94
AKTDHGAEIVYKSPVVSGDTSPR-KVAVVRTPPK-a12-b1	TAU_HUMAN P10636-8	TAU_HUMAN P10636-8	xlink	ntra-protein ›	395	225	170	3645.003	912.259	4	3.8	14.62
EPKKVAVVR-LDFKDR-a3-b4	TAU_HUMAN P10636-8	TAU_HUMAN P10636-8	xlink	ntra-protein ›	224	347	123	1955.111	652.711	3	-4.9	13.25
AKTDHGAEIVYKSPVVSGDTSPR-KVAVVRTPPK-a2-b1	TAU_HUMAN P10636-8	TAU_HUMAN P10636-8	xlink	ntra-protein ›	385	225	160	3645.003	912.259	4	3.8	12.98
EPKKVAVVR-LDFKDR-a4-b4	TAU_HUMAN P10636-8	TAU_HUMAN P10636-8	xlink	ntra-protein ›	225	347	122	1955.111	652.711	3	-4.9	12.25
TPPKSPSSAKSR-KIETHKLTFR-a10-b6	TAU_HUMAN P10636-8	TAU_HUMAN P10636-8	xlink	ntra-protein ›	240	375	135	2651.475	663.877	4	-0.3	10.79
KLDLSNVQSK-TKIATPR-a1-b2	TAU_HUMAN P10636-8	TAU_HUMAN P10636-8	xlink	ntra-protein ›	281	150	131	2054.18	685.735	3	3.3	10.38

Mh XL-MS Data

Id	Protein1	Protein2	Type	XLType	AbsPos1	AbsPos2	deltaAA	Mr	Mz	z	Error_rel[ppm]	Id-Score
VQSKIGSLDNITHVPGGGNK-SEKLDFKDR-a4-b7	TAU_HUMAN P10636-8	TAU_HUMAN P10636-8	xlink	ntra-protein ›	353	347	6	3294.737	824.692	4	4.8	44.77
VQSKIGSLDNITHVPGGGNK-SEKLDFKDR-a4-b3	TAU_HUMAN P10636-8	TAU_HUMAN P10636-8	xlink	ntra-protein ›	353	343	10	3294.736	824.692	4	4.7	44.15
IGSLDNITHVPGGGNKK-IETHKLTFR-a16-b5	TAU_HUMAN P10636-8	TAU_HUMAN P10636-8	xlink	ntra-protein ›	369	375	6	2987.631	747.916	4	4.1	43.9
IGSTENLKHQPGGGK-VQIINKK-a8-b6	TAU_HUMAN P10636-8	TAU_HUMAN P10636-8	xlink	ntra-protein ›	267	280	13	2501.408	834.811	3	4.7	41.5
AKTDHGAEIVYK-IETHKLTFR-a2-b5	TAU_HUMAN P10636-8	TAU_HUMAN P10636-8	xlink	ntra-protein ›	385	375	10	2612.405	654.109	4	3.5	41.19
IGSLDNITHVPGGGNKK-AKTDHGAEIVYK-a16-b2	TAU_HUMAN P10636-8	TAU_HUMAN P10636-8	xlink	ntra-protein ›	369	385	16	3174.679	794.678	4	3.8	41
TDHGAEIVYKSPVVSGDTSPR-ENAKAK-a10-b4	TAU_HUMAN P10636-8	TAU_HUMAN P10636-8	xlink	ntra-protein ›	395	383	12	3011.535	603.315	5	4.9	40.77
VQSKIGSLDNITHVPGGGNK-LDFKDR-a4-b4	TAU_HUMAN P10636-8	TAU_HUMAN P10636-8	xlink	ntra-protein ›	353	347	6	2950.565	591.121	5	4.8	39.59
SKDGTGSDDKK-TKIATPR-a2-b2	TAU_HUMAN P10636-8	TAU_HUMAN P10636-8	xlink	ntra-protein ›	132	150	18	2060.082	516.028	4	3.4	39.26
AKGADGK-TKIATPR-a2-b2	TAU_HUMAN P10636-8	TAU_HUMAN P10636-8	xlink	ntra-protein ›	143	150	7	1568.892	393.231	4	2.1	39.24
LDLSNVQSKAGSK-VQIINKK-a9-b6	TAU_HUMAN P10636-8	TAU_HUMAN P10636-8	xlink	ntra-protein ›	290	280	10	2325.337	582.342	4	4.5	38.61
AKGADGK-TKIATPR-a2-b2	TAU_HUMAN P10636-8	TAU_HUMAN P10636-8	xlink	ntra-protein ›	143	150	7	1568.893	393.231	4	3.1	38.24
IPAKTPPAPK-TKIATPR-a4-b2	TAU_HUMAN P10636-8	TAU_HUMAN P10636-8	xlink	ntra-protein ›	174	150	24	1942.17	486.55	4	4.5	37.76
KLDLSNVQSK-AGSKDNIK-a1-b4	TAU_HUMAN P10636-8	TAU_HUMAN P10636-8	xlink	ntra-protein ›	281	294	13	2100.152	701.058	3	4.4	37.75
IGSLDNITHVPGGGNKK-IETHKLTFR-a16-b5	TAU_HUMAN P10636-8	TAU_HUMAN P10636-8	xlink	ntra-protein ›	369	375	6	2987.633	747.916	4	4.6	37.09
VQSKIGSLDNITHVPGGGNKK-LDFKDR-a4-b4	TAU_HUMAN P10636-8	TAU_HUMAN P10636-8	xlink	ntra-protein ›	353	347	6	3078.657	616.739	5	3.5	36.99
GAAPPGQKGQANATR-GADGKTK-a8-b5	TAU_HUMAN P10636-8	TAU_HUMAN P10636-8	xlink	ntra-protein ›	163	148	15	2236.164	560.049	4	3.7	36.57
SKDGTGSDDKK-GADGKTK-a10-b5	TAU_HUMAN P10636-8	TAU_HUMAN P10636-8	xlink	ntra-protein ›	140	148	8	1949.962	650.995	3	3.9	36.56
SKDGTGSDDKK-TKIATPR-a10-b2	TAU_HUMAN P10636-8	TAU_HUMAN P10636-8	xlink	ntra-protein ›	140	150	10	2060.083	687.702	3	3.7	35.7
IGSTENLKHQPGGGK-KLDLSNVQSK-a8-b1	TAU_HUMAN P10636-8	TAU_HUMAN P10636-8	xlink	ntra-protein ›	267	281	14	2790.5	698.633	4	4.6	35.64
HQPGGGKVQIINK-KLDLSNVQSK-a7-b1	TAU_HUMAN P10636-8	TAU_HUMAN P10636-8	xlink	ntra-protein ›	274	281	7	2643.48	529.704	5	3.5	35.13
IETHKLTFR-SEKLDFKDR-a5-b3	TAU_HUMAN P10636-8	TAU_HUMAN P10636-8	xlink	ntra-protein ›	375	343	32	2418.297	484.667	5	2.5	34.61
AKTDHGAEIVYK-KIETHKLTFR-a2-b6	TAU_HUMAN P10636-8	TAU_HUMAN P10636-8	xlink	ntra-protein ›	385	375	10	2740.501	686.133	4	3.5	34.09
AKTDHGAEIVYK-SEKLDFKDR-a2-b7	TAU_HUMAN P10636-8	TAU_HUMAN P10636-8	xlink	ntra-protein ›	385	347	38	2605.351	652.346	4	4.8	34.04
AGSKDNIK-VQIINKK-a4-b6	TAU_HUMAN P10636-8	TAU_HUMAN P10636-8	xlink	ntra-protein ›	294	280	14	1811.06	604.695	3	4.9	33.37
IPAKTPPAPK-TKIATPR-a4-b2	TAU_HUMAN P10636-8	TAU_HUMAN P10636-8	xlink	ntra-protein ›	174	150	24	1942.169	486.55	4	3.7	33.21
VQSKIGSLDNITHVPGGGNK-KIETHK-a4-b1	TAU_HUMAN P10636-8	TAU_HUMAN P10636-8	xlink	ntra-protein ›	353	370	17	2912.585	971.87	3	4.5	33.12
GAAPPGQKGQANATR-SKDGTGSDDKK-a8-b2	TAU_HUMAN P10636-8	TAU_HUMAN P10636-8	xlink	ntra-protein ›	163	132	31	2697.344	675.344	4	4.4	32.9
SKDGTGSDDKK-AKGADGK-a10-b2	TAU_HUMAN P10636-8	TAU_HUMAN P10636-8	xlink	ntra-protein ›	140	143	3	1919.951	640.992	3	4	32.84
AKGADGK-XVSKSK-a2-b4	TAU_HUMAN P10636-8	TAU_HUMAN P10636-8	xlink	ntra-protein ›	143	130	13	1477.786	493.603	3	3.7	32.58
TPPKSPSSAK-KVAVVR-a4-b1	TAU_HUMAN P10636-8	TAU_HUMAN P10636-8	xlink	ntra-protein ›	234	225	9	1807.063	452.774	4	3.3	32.07
HQPGGGKVQIINK-SKIGSTENLK-a7-b2	TAU_HUMAN P10636-8	TAU_HUMAN P10636-8	xlink	ntra-protein ›	274	259	15	2588.442	648.118	4	5	32.06
DGTGSDDKK-MVSKSK-a8-b4	TAU_HUMAN P10636-8	TAU_HUMAN P10636-8	xlink	ntra-protein ›	140	130	10	1737.851	580.291	3	2.9	32.05
HQPGGGKVQIINK-SKIGSTENLK-a7-b2	TAU_HUMAN P10636-8	TAU_HUMAN P10636-8	xlink	ntra-protein ›	274	259	15	2588.441	648.118	4	4.7	31.96
SKDGTGSDDKK-AKGADGK-a2-b2	TAU_HUMAN P10636-8	TAU_HUMAN P10636-8	xlink	ntra-protein ›	132	143	11	1919.953	480.996	4	5	31.82
KLDLSNVQSK-SKIGSTENLK-a1-b2	TAU_HUMAN P10636-8	TAU_HUMAN P10636-8	xlink	ntra-protein ›	281	259	22	2344.296	587.082	4	4.5	31.43
VQSKIGSLDNITHVPGGGNK-KIETHK-a4-b1	TAU_HUMAN P10636-8	TAU_HUMAN P10636-8	xlink	ntra-protein ›	353	370	17	2912.584	583.525	5	4.2	31.1
AKTDHGAEIVYK-LDFKDR-a2-b4	TAU_HUMAN P10636-8	TAU_HUMAN P10636-8	xlink	ntra-protein ›	385	347	38	2261.178	566.302	4	3.9	30.85
SKDGTGSDDKK-TKIATPR-a10-b2	TAU_HUMAN P10636-8	TAU_HUMAN P10636-8	xlink	ntra-protein ›	140	150	10	2060.085	687.703	3	4.9	30.84
TPPKSPSSAKSR-KVAVVR-a10-b1	TAU_HUMAN P10636-8	TAU_HUMAN P10636-8	xlink	ntra-protein ›	240	225	15	2050.197	513.557	4	3.6	30.28
IGSLDNITHVPGGGNKK-LDFKDR-a16-b4	TAU_HUMAN P10636-8	TAU_HUMAN P10636-8	xlink	ntra-protein ›	369	347	22	2636.399	528.288	5	2.6	30.17
TKIATPR-XVSKSK-a2-b4	TAU_HUMAN P10636-8	TAU_HUMAN P10636-8	xlink	ntra-protein ›	150	130	20	1617.919	540.314	3	4.3	30.13
IGSLDNITHVPGGGNKK-SEKLDFKDR-a16-b3	TAU_HUMAN P10636-8	TAU_HUMAN P10636-8	xlink	ntra-protein ›	369	343	26	2980.576	746.152	4	4.7	30.09
HQPGGGKVQIINK-KLDLSNVQSK-a7-b1	TAU_HUMAN P10636-8	TAU_HUMAN P10636-8	xlink	ntra-protein ›	274	281	7	2643.478	882.167	3	2.8	29.9
GAAPPGQKGQANATR-IPAKTPPAPK-a8-b4	TAU_HUMAN P10636-8	TAU_HUMAN P10636-8	xlink	ntra-protein ›	163	174	11	2579.43	645.865	4	4.6	29.82
TPPKSPSSAKSR-KVAVVR-a10-b1	TAU_HUMAN P10636-8	TAU_HUMAN P10636-8	xlink	ntra-protein ›	240	225	15	2050.199	513.558	4	4.3	28.62
SKDGTGSDDKK-IPAKTPPAPK-a10-b4	TAU_HUMAN P10636-8	TAU_HUMAN P10636-8	xlink	ntra-protein ›	140	174	34	2293.224	765.416	3	3.4	28.6
ESPLQTPTEDGSEEPGSETSDAKSTPTAEDVTAPLVDEGAPGK	TAU_HUMAN P10636-8	TAU_HUMAN P10636-8	xlink	ntra-protein ›	67	150	83	5249.534	1313.391	4	4.3	28.05
DGTGSDDKK-GADGKTK-a8-b5	TAU_HUMAN P10636-8	TAU_HUMAN P10636-8	xlink	ntra-protein ›	140	148	8	1734.835	579.286	3	4.8	27.52
HVPGGGSVQIVYKPVDLSK-KLDLSNVQSK-a13-b1	TAU_HUMAN P10636-8	TAU_HUMAN P10636-8	xlink	ntra-protein ›	311	281	30	3247.794	812.956	4	3.7	26.9
IGSTENLKHQPGGGK-VQIINKK-a8-b6	TAU_HUMAN P10636-8	TAU_HUMAN P10636-8	xlink	ntra-protein ›	267	280	13	2501.409	626.36	4	5	26.77
TPPKSPSSAK-KVAVVR-a4-b1	TAU_HUMAN P10636-8	TAU_HUMAN P10636-8	xlink	ntra-protein ›	234	225	9	1807.063	452.774	4	3.5	26.66
DGTGSDDKKAK-TKIATPR-a8-b2	TAU_HUMAN P10636-8	TAU_HUMAN P10636-8	xlink	ntra-protein ›	140	150	10	2044.087	512.03	4	3.5	26.48
SKDGTGSDDKK-GADGKTK-a10-b5	TAU_HUMAN P10636-8	TAU_HUMAN P10636-8	xlink	ntra-protein ›	140	148	8	1949.961	488.498	4	3.5	26.09
GAAPPGQKGQANATR-SKDGTGSDDKK-a8-b10	TAU_HUMAN P10636-8	TAU_HUMAN P10636-8	xlink	ntra-protein ›	163	140	23	2697.345	900.123	3	4.7	25.97
GAAPPGQKGQANATR-TKIATPR-a8-b2	TAU_HUMAN P10636-8	TAU_HUMAN P10636-8	xlink	ntra-protein ›	163	150	13	2346.287	783.104	3	4.5	25.82
DGTGSDDKKAK-XVSKSK-a8-b4	TAU_HUMAN P10636-8	TAU_HUMAN P10636-8	xlink	ntra-protein ›	140	130	10	1952.981	489.253	4	4.3	25.22

Mr XL-MS Data

Id	Protein1	Protein2	Type	XLType	AbsPos1	AbsPos2	deltaAA	Mr	Mz	z	Error_rel[ppm]	Id-Score
TDHGAEIVYKSPVVSGDTSPR-ENAKAK-a10-b4	TAU_HUMAN P10636-8	TAU_HUMAN P10636-8	xlink	intra-protein xl	395	383	12	3011.526	603.313	5	2.1	44.8
IGSLDNITHVPGGGNKK-IETHKLTFR-a16-b5	TAU_HUMAN P10636-8	TAU_HUMAN P10636-8	xlink	intra-protein xl	369	375	6	2987.63	747.915	4	3.5	44.11
AKTDHGAEIVYK-IETHKLTFR-a2-b5	TAU_HUMAN P10636-8	TAU_HUMAN P10636-8	xlink	intra-protein xl	385	375	10	2612.405	654.109	4	3.5	43.76
LDLSNVQSKAGSK-VQIINKK-a9-b6	TAU_HUMAN P10636-8	TAU_HUMAN P10636-8	xlink	intra-protein xl	290	280	10	2325.333	582.341	4	2.8	42.56
IPAKTPPAPK-TKIATPR-a4-b2	TAU_HUMAN P10636-8	TAU_HUMAN P10636-8	xlink	intra-protein xl	174	150	24	1942.165	486.549	4	1.8	39.78
IGSLDNITHVPGGGNKK-AKTDHGAEIVYK-a16-b2	TAU_HUMAN P10636-8	TAU_HUMAN P10636-8	xlink	intra-protein xl	369	385	16	3174.676	794.677	4	2.8	39.35
AKGADGK-TKIATPR-a2-b2	TAU_HUMAN P10636-8	TAU_HUMAN P10636-8	xlink	intra-protein xl	143	150	7	1568.891	523.971	3	1.3	37.95
IPAKTPPAPK-TKIATPR-a4-b2	TAU_HUMAN P10636-8	TAU_HUMAN P10636-8	xlink	intra-protein xl	174	150	24	1942.167	486.549	4	2.6	37.35
AGSLGNIHHKPGGGQVEVK-SEKLDFKDR-a10-b3	TAU_HUMAN P10636-8	TAU_HUMAN P10636-8	xlink	intra-protein xl	331	343	12	3158.654	632.739	5	2.3	37.34
AKTDHGAEIVYK-IETHKLTFR-a2-b5	TAU_HUMAN P10636-8	TAU_HUMAN P10636-8	xlink	intra-protein xl	385	375	10	2612.402	654.108	4	2.3	35.62
KLDLSNVQSK-SKIGSTENLK-a1-b2	TAU_HUMAN P10636-8	TAU_HUMAN P10636-8	xlink	intra-protein xl	281	259	22	2344.293	587.081	4	3.4	34.51
HVPGGGSVQIVYKPVDLSK-KLDLSNVQSK-a13-b1	TAU_HUMAN P10636-8	TAU_HUMAN P10636-8	xlink	intra-protein xl	311	281	30	3247.792	812.956	4	3.2	34.32
AKGADGK-TKIATPR-a2-b2	TAU_HUMAN P10636-8	TAU_HUMAN P10636-8	xlink	intra-protein xl	143	150	7	1568.892	523.972	3	2	34.2
KLDLSNVQSK-AGSKDNIK-a1-b4	TAU_HUMAN P10636-8	TAU_HUMAN P10636-8	xlink	intra-protein xl	281	294	13	2100.149	701.057	3	2.9	33.36
AGSLGNIHHKPGGGQVEVK-HVPGGGSVQIVYKPVDLSK-a10-b13	TAU_HUMAN P10636-8	TAU_HUMAN P10636-8	xlink	intra-protein xl	331	311	20	4001.161	801.24	5	3	32.15
TPPKSPSSAK-KVAVVR-a4-b1	TAU_HUMAN P10636-8	TAU_HUMAN P10636-8	xlink	intra-protein xl	234	225	9	1807.06	452.773	4	1.7	31.88
GAAPPGQKGQANATR-TKIATPR-a8-b2	TAU_HUMAN P10636-8	TAU_HUMAN P10636-8	xlink	intra-protein xl	163	150	13	2346.28	587.578	4	1.2	31.51
VQSKIGSLDNITHVPGGGNK-LDFKDR-a4-b4	TAU_HUMAN P10636-8	TAU_HUMAN P10636-8	xlink	intra-protein xl	353	347	6	2950.562	738.648	4	3.8	30.41
DNIKHVPGGGSVQIVYKPVDLSK-LDLSNVQSKAGSK-a4-b9	TAU_HUMAN P10636-8	TAU_HUMAN P10636-8	xlink	intra-protein xl	298	290	8	3933.131	787.634	5	2.6	30.29
GAAPPGQKGQANATR-TKIATPR-a8-b2	TAU_HUMAN P10636-8	TAU_HUMAN P10636-8	xlink	intra-protein xl	163	150	13	2346.285	587.579	4	3.6	30.2
TDHGAEIVYKSPVVSGDTSPR-LDFKDR-a10-b4	TAU_HUMAN P10636-8	TAU_HUMAN P10636-8	xlink	intra-protein xl	395	347	48	3144.582	787.153	4	2.9	29.63
VQSKIGSLDNITHVPGGGNK-AGSLGNIHHKPGGGQVEVK-a4-b10	TAU_HUMAN P10636-8	TAU_HUMAN P10636-8	xlink	intra-protein xl	353	331	22	4042.146	1011.544	4	2.8	28.7
HVPGGGSVQIVYKPVDLSK-SKIGSTENLK-a13-b2	TAU_HUMAN P10636-8	TAU_HUMAN P10636-8	xlink	intra-protein xl	311	259	52	3192.749	799.195	4	2.9	28.45
TDHGAEIVYKSPVVSGDTSPR-ENAKAK-a10-b4	TAU_HUMAN P10636-8	TAU_HUMAN P10636-8	xlink	intra-protein xl	395	383	12	3011.53	603.314	5	3.3	27.63
IGSLDNITHVPGGNKK-IETHKLTFR-a16-b5	TAU_HUMAN P10636-8	TAU_HUMAN P10636-8	xlink	intra-protein xl	369	375	6	2987.627	747.915	4	2.6	26.31

Control1 XL-MS Data

Id	Protein1	Protein2	Type	XLType	AbsPos1	AbsPos2	deltaAA	Mr	Mz	z	Error_rel[ppm]	ld-Score
GAAPPGQKGQANATR-TKIATPR-a8-b2	TAU_HUMAN P10636-8	TAU_HUMAN P10636-8	xlink	intra-protein xl	163	150	13	2346.281	783.101	3	1.8	23.18
TPSLPTPPTREPKK-TKIATPR-a13-b2	TAU_HUMAN P10636-8	TAU_HUMAN P10636-8	xlink	intra-protein xl	224	150	74	2471.411	618.86	4	-0.2	11.94
CGSLGNIHHKPGGGQVEVKSEK-CGSKDNIX-a19-b4	TAU_HUMAN P10636-8	TAU_HUMAN P10636-8	xlink	intra-protein xl	340	294	46	3489.717	873.437	4	2.2	10.85
AKTDHGAEIVYK-MVSKSK-a2-b4	TAU_HUMAN P10636-8	TAU_HUMAN P10636-8	xlink	intra-protein xl	385	130	255	2147.124	716.716	3	-2.8	9.39
IGSLDNITHVPGGGNKK-SKIGSTENLX-a16-b2	TAU_HUMAN P10636-8	TAU_HUMAN P10636-8	xlink	intra-protein xl	369	259	110	3033.611	1012.212	3	0.5	7.13

Control2 XL-MS Data

Id	Protein1	Protein2	Type	XLType	AbsPos1	AbsPos2	deltaAA	Mr	Mz	z	Error_rel[ppm]	Id-Score
SEKLDFK-KVAVVR-a3-b1	TAU_HUMAN P10636-8	TAU_HUMAN P10636-8	xlink	intra-protein xl	343	225	118	1673.972	558.999	3	0.3	15.16
LTFRENAKAX-SEKLDFXDR-a8-b3	TAU_HUMAN P10636-8	TAU_HUMAN P10636-8	xlink	intra-protein xl	383	343	40	2679.409	670.86	4	4	9.85
IPAKTPPAPK-TKIATPR-a4-b2	TAU_HUMAN P10636-8	TAU_HUMAN P10636-8	xlink	intra-protein xl	174	150	24	1942.156	648.393	3	-2.7	8.99
TPPAPXTPPSSGEPPKSGDR-IGSLDNITHVPGGGNKK-a16-b16	TAU_HUMAN P10636-8	TAU_HUMAN P10636-8	xlink	intra-protein xl	190	369	179	3960.039	991.018	4	1.2	8.05
IETHKLTFR-AKGADGX-a5-b2	TAU_HUMAN P10636-8	TAU_HUMAN P10636-8	xlink	intra-protein xl	375	143	232	2041.086	681.37	3	-5	7.29

Control3 XL-MS Data

Id	Protein1	Protein2	Type	XLType	AbsPos1	AbsPos2	deltaAA	Mr	Mz	z	Error_rel[ppm]	Id-Score
GAAPPGQKGQANATR-TKIATPR-a8-b2	TAU_HUMAN P10636-8	TAU_HUMAN P10636-8	xlink	intra-protein	163	150	13	2346.279	783.101	3	0.8	13.51
SPSSAKSRLQTAPVPMPDLK-KAKGADGK-a6-b3	TAU_HUMAN P10636-8	TAU_HUMAN P10636-8	xlink	intra-protein	240	143	97	3020.641	605.136	5	2.7	11.95
DGTGSDDKKAK-KVAVVR-a9-b1	TAU_HUMAN P10636-8	TAU_HUMAN P10636-8	xlink	intra-protein	141	225	84	1929.056	644.026	3	1.3	11.75
CGSKDNIK-SPSSAKSR-a4-b6	TAU_HUMAN P10636-8	TAU_HUMAN P10636-8	xlink	intra-protein	294	240	54	1876.928	626.651	3	-1.7	11.49
TPPAPKTPPSSGEPPX-HQPGGGKVQIINK-a6-b7	TAU_HUMAN P10636-8	TAU_HUMAN P10636-8	xlink	intra-protein	180	274	94	3213.702	1072.242	3	-4	9.08
SKDGTGSDDKK-SEKLDFKDR-a10-b3	TAU_HUMAN P10636-8	TAU_HUMAN P10636-8	xlink	intra-protein	140	343	203	2411.182	603.803	4	0.1	8.39
SKDGTGSDDKK-SEKLDFKDR-a2-b3	TAU_HUMAN P10636-8	TAU_HUMAN P10636-8	xlink	intra-protein	132	343	211	2411.184	603.804	4	1	7.43

AD1 XL-MS Data

Id	Protein1	Protein2	Type	XLType	AbsPos1	AbsPos2	deltaAA	Mr	Mz	z	Error_rel[ppm]	Id-Score
GAAPPGQKGQANATR-IPAKTPPAPK-a8-b4	TAU_HUMAN P10636-8	TAU_HUMAN P10636-8	xlink	ntra-protein ›	163	174	11	2579.42	645.863	4	0.8	20.56
LTFRENAKAK-EPXKVAVVR-a8-b4	TAU_HUMAN P10636-8	TAU_HUMAN P10636-8	xlink	ntra-protein ›	383	225	158	2453.415	614.362	4	1.2	14.55
CGSKDNIK-ENAKAX-a4-b4	TAU_HUMAN P10636-8	TAU_HUMAN P10636-8	xlink	ntra-protein ›	294	383	89	1831.908	458.985	4	-1.1	14.08
AKGADGK-SEKLDFK-a2-b3	TAU_HUMAN P10636-8	TAU_HUMAN P10636-8	xlink	ntra-protein ›	143	343	200	1648.871	550.632	3	2.6	10.23
GAAPPGQKGQANATR-SPSSAKSR-a8-b6	TAU_HUMAN P10636-8	TAU_HUMAN P10636-8	xlink	ntra-protein ›	163	240	77	2379.218	595.812	4	-3.1	9.07
AKGADGKTK-KIETHX-a7-b1	TAU_HUMAN P10636-8	TAU_HUMAN P10636-8	xlink	ntra-protein ›	148	370	222	1881.033	628.019	3	0.7	8.48
DGTGSDDKX-KIETHX-a8-b1	TAU_HUMAN P10636-8	TAU_HUMAN P10636-8	xlink	ntra-protein ›	140	370	230	2041.987	681.67	3	-2.4	8.28
SKIGSTENLX-TKIATPR-a2-b2	TAU_HUMAN P10636-8	TAU_HUMAN P10636-8	xlink	ntra-protein ›	259	150	109	2113.166	705.396	3	-4	8.02
GADGKTKIATPR-SEKLDFKDR-a5-b3	TAU_HUMAN P10636-8	TAU_HUMAN P10636-8	xlink	ntra-protein ›	148	343	195	2488.329	623.09	4	0.4	8.01
LQTAPVPMPDLKNVKSK-SKDGTGSDDKX-a15-b2	TAU_HUMAN P10636-8	TAU_HUMAN P10636-8	xlink	ntra-protein ›	257	132	125	3253.7	1085.574	3	4	7.26
IETHKLTFR-AKGADGX-a5-b2	TAU_HUMAN P10636-8	TAU_HUMAN P10636-8	xlink	ntra-protein ›	375	143	232	2041.088	681.37	3	-4	7.14

AD2 XL-MS Data

Id	Protein1	Protein2	Type	XLType	AbsPos1	AbsPos2	deltaAA	Mr	Mz	z	Error_rel[ppm]	Id-Score
SEKLDFK-KVAVVR-a3-b1	TAU_HUMAN P10636-8	TAU_HUMAN P10636-8	xlink	ntra-protein ›	343	225	118	1673.972	558.999	3	0.4	13.67
KLDLSNVQSK-SPSSAKSR-a1-b6	TAU_HUMAN P10636-8	TAU_HUMAN P10636-8	xlink	ntra-protein ›	281	240	41	2087.127	696.717	3	2.2	12.28
IETHKLTFR-AKGADGX-a5-b2	TAU_HUMAN P10636-8	TAU_HUMAN P10636-8	xlink	ntra-protein ›	375	143	232	2041.088	681.371	3	-3.6	9.9
NVKSKIGSTENLX-SPSSAKSR-a5-b6	TAU_HUMAN P10636-8	TAU_HUMAN P10636-8	xlink	ntra-protein ›	259	240	19	2487.328	622.84	4	-0.5	9.49
IGSLDNITHVPGGGNKX-TPPSSGEPPKSGDR-a16-b10	TAU_HUMAN P10636-8	TAU_HUMAN P10636-8	xlink	ntra-protein ›	369	190	179	3368.695	843.182	4	-0.3	8.92
IGSTENLKHQPGGGKVQIINX-LTFRENAKAX-a15-b8	TAU_HUMAN P10636-8	TAU_HUMAN P10636-8	xlink	ntra-protein ›	274	383	109	3760.031	941.015	4	-2.1	8.59
GADGKTKIATPR-VQIINKK-a7-b6	TAU_HUMAN P10636-8	TAU_HUMAN P10636-8	xlink	ntra-protein ›	150	280	130	2193.278	732.1	3	-3.2	7.7
SKDGTGSDDKX-LDFKDRVQSX-a10-b4	TAU_HUMAN P10636-8	TAU_HUMAN P10636-8	xlink	ntra-protein ›	140	347	207	2737.345	913.456	3	-2.6	7.63
SRLQTAPVPMPDLKNVK-SKDGTGSDDKX-a14-b10	TAU_HUMAN P10636-8	TAU_HUMAN P10636-8	xlink	ntra-protein ›	254	140	114	3281.68	821.428	4	-4	7.05
SRLQTAPVPMPDLKNVX-SKDGTGSDDKK-a14-b2	TAU_HUMAN P10636-8	TAU_HUMAN P10636-8	xlink	ntra-protein ›	254	132	122	3281.677	821.427	4	-4.6	7.03

AD3 XL-MS Data

Id	Protein1	Protein2	Type	XLType	AbsPos1	AbsPos2	deltaAA	Mr	Mz	z	Error_rel[ppm]	Id-Score
GQANATRIPAKTPPAPK-KAKGADGK-a11-b3	TAU_HUMAN P10636-8	TAU_HUMAN P10636-8	xlink	ntra-protein ›	174	143	31	2628.463	877.162	3	-2.9	11.1
SEKLDFK-KVAVVR-a3-b1	TAU_HUMAN P10636-8	TAU_HUMAN P10636-8	xlink	ntra-protein ›	343	225	118	1673.971	558.998	3	-0.1	9.73
AKTDHGAEIVYK-KIETHK-a2-b1	TAU_HUMAN P10636-8	TAU_HUMAN P10636-8	xlink	ntra-protein ›	385	370	15	2223.196	742.073	3	2.9	9.47
TKIATPRGAAPPGQX-SKDGTGSDDKK-a2-b2	TAU_HUMAN P10636-8	TAU_HUMAN P10636-8	xlink	ntra-protein ›	150	132	18	2880.49	961.171	3	-1.3	8.88
EPXKVAVVR-GADGKTX-a4-b5	TAU_HUMAN P10636-8	TAU_HUMAN P10636-8	xlink	ntra-protein ›	225	148	77	2066.156	689.727	3	3.8	8.07
TPPKSPSSAX-KAKGADGX-a4-b1	TAU_HUMAN P10636-8	TAU_HUMAN P10636-8	xlink	ntra-protein ›	234	141	93	2138.126	713.717	3	-3.2	7.89
SPSSAKSRLQTAPVPMPDLK-KAKGADGK-a6-b3	TAU_HUMAN P10636-8	TAU_HUMAN P10636-8	xlink	ntra-protein ›	240	143	97	3020.646	756.169	4	4.2	7.7
DRVQSKIGSLDNITHVPGGGNK-SKIGSTENLKHQPGGGK-a6-b10	TAU_HUMAN P10636-8	TAU_HUMAN P10636-8	xlink	ntra-protein ›	353	267	86	4166.169	1042.55	4	-3.3	7.57
KLDLSNVQSKCGSX-AKGADGKTK-a10-b7	TAU_HUMAN P10636-8	TAU_HUMAN P10636-8	xlink	ntra-protein ›	290	148	142	2689.407	897.477	3	-0.1	7.52
KDQGGYTMHQDQEGDTDAGLK-VQSKIGSLDNITHVPGGGNK-a1-b4	TAU_HUMAN P10636-8	TAU_HUMAN P10636-8	xlink	ntra-protein ›	24	353	329	4451.124	1113.789	4	-1.2	7.35
TPPKSPSSAXSR-CGSKDNIK-a4-b4	TAU_HUMAN P10636-8	TAU_HUMAN P10636-8	xlink	ntra-protein ›	234	294	60	2414.217	805.747	3	-2.2	7.34
KLDLSNVQSKCGSK-TKIATPR-a1-b2	TAU_HUMAN P10636-8	TAU_HUMAN P10636-8	xlink	ntra-protein ›	281	150	131	2486.346	829.79	3	-2.7	7.3
SKIGSTENLK-SEKLDFKDR-a2-b7	TAU_HUMAN P10636-8	TAU_HUMAN P10636-8	xlink	ntra-protein ›	259	347	88	2350.243	784.422	3	2.2	7

Dounce Homogenization XL-MS Data

Id	Protein1	Protein2	Type	XLType	AbsPos1	AbsPos2	deltaAA	Mr	Mz	z	Error_rel[ppm]	Id-Score
GADGKTX-ENAKAX-a5-b4	TAU_HUMAN P10636-8	TAU_HUMAN P10636-8	xlink	intra-protein xl	148	383	235	1700.872	567.965	3	1.5	10.92
DGTGSDDKX-KIETHX-a8-b1	TAU_HUMAN P10636-8	TAU_HUMAN P10636-8	xlink	intra-protein xl	140	370	230	2041.988	681.67	3	-2.1	10.39
SKIGSTENLX-TKIATPR-a2-b2	TAU_HUMAN P10636-8	TAU_HUMAN P10636-8	xlink	intra-protein xl	259	150	109	2113.165	705.396	3	-4.6	8.05

Mechanical Homogenization XL-MS Data

Id	Protein1	Protein2	Type	XLType	AbsPos1	AbsPos2	deltaAA	Mr	Mz	z	Error_rel[ppm]	Id-Score
VQSKIGSLDNITHVPGGGNK-SEKLDFKDR-a4-b3	TAU_HUMAN P10636-8	TAU_HUMAN P10636-8	xlink	intra-protein xl	353	343	10	3294.726	824.689	4	1.5	44.99
HQPGGGKVQIINK-KLDLSNVQSK-a7-b1	TAU_HUMAN P10636-8	TAU_HUMAN P10636-8	xlink	intra-protein xl	274	281	7	2643.47	529.702	5	-0.4	41.49
VQSKIGSLDNITHVPGGGNK-VQIINKK-a4-b6	TAU_HUMAN P10636-8	TAU_HUMAN P10636-8	xlink	intra-protein xl	353	280	73	2999.684	1000.902	3	2.3	40.96
VTSKCGSLGNIHHKPGGGQVEVK-KLDLSNVQSK-a4-b1	TAU_HUMAN P10636-8	TAU_HUMAN P10636-8	xlink	intra-protein xl	321	281	40	3656.922	1219.982	3	-2.3	40.46
IGSLDNITHVPGGGNKK-LDFKDR-a16-b4	TAU_HUMAN P10636-8	TAU_HUMAN P10636-8	xlink	intra-protein xl	369	347	22	2636.398	660.107	4	2.2	39.99
VTSKCGSLGNIHHKPGGGQVEVK-SEKLDFK-a4-b3	TAU_HUMAN P10636-8	TAU_HUMAN P10636-8	xlink	intra-protein xl	321	343	22	3391.757	679.359	5	0.3	39.92
KLDLSNVQSK-SKIGSTENLK-a1-b2	TAU_HUMAN P10636-8	TAU_HUMAN P10636-8	xlink	intra-protein xl	281	259	22	2344.288	782.437	3	1.3	39.69
IGSTENLKHQPGGGK-KLDLSNVQSK-a8-b1	TAU_HUMAN P10636-8	TAU_HUMAN P10636-8	xlink	intra-protein xl	267	281	14	2790.485	931.169	3	-1	39.44
IGSLDNITHVPGGGNKK-SEKLDFKDR-a16-b3	TAU_HUMAN P10636-8	TAU_HUMAN P10636-8	xlink	intra-protein xl	369	343	26	2980.565	746.149	4	1	39.26
DNIKHVPGGGSVQIVYKPVDLSK-VQIINKK-a4-b6	TAU_HUMAN P10636-8	TAU_HUMAN P10636-8	xlink	intra-protein xl	298	280	18	3428.937	572.497	6	-0.9	38.63
LDLSNVQSKCGSK-SKIGSTENLK-a9-b2	TAU_HUMAN P10636-8	TAU_HUMAN P10636-8	xlink	intra-protein xl	290	259	31	2648.372	883.799	3	1.2	38.54
VQSKIGSLDNITHVPGGGNK-SKIGSTENLK-a4-b2	TAU_HUMAN P10636-8	TAU_HUMAN P10636-8	xlink	intra-protein xl	353	259	94	3233.727	1078.917	3	0.6	38.53
LDLSNVQSKCGSK-VQIINKK-a9-b6	TAU_HUMAN P10636-8	TAU_HUMAN P10636-8	xlink	intra-protein xl	290	280	10	2414.319	604.588	4	-0.4	37.82
DNIKHVPGGGSVQIVYKPVDLSK-KLDLSNVQSK-a4-b1	TAU_HUMAN P10636-8	TAU_HUMAN P10636-8	xlink	intra-protein xl	298	281	17	3718.026	620.679	6	-1.1	37.54
KLDLSNVQSK-LDFKDR-a1-b4	TAU_HUMAN P10636-8	TAU_HUMAN P10636-8	xlink	intra-protein xl	281	347	66	2061.112	688.045	3	0.6	37.04
VQIINKK-LDFKDR-a6-b4	TAU_HUMAN P10636-8	TAU_HUMAN P10636-8	xlink	intra-protein xl	280	347	67	1772.017	444.012	4	-1.5	36.8
HVPGGGSVQIVYKPVDLSK-SEKLDFK-a13-b3	TAU_HUMAN P10636-8	TAU_HUMAN P10636-8	xlink	intra-protein xl	311	343	32	2982.609	746.66	4	0.8	36.29
VQSKIGSLDNITHVPGGGNK-LDFKDR-a4-b4	TAU_HUMAN P10636-8	TAU_HUMAN P10636-8	xlink	intra-protein xl	353	347	6	2950.557	738.647	4	1.9	36.04
VTSKCGSLGNIHHKPGGGQVEVK-LDFKDR-a4-b4	TAU_HUMAN P10636-8	TAU_HUMAN P10636-8	xlink	intra-protein xl	321	347	26	3318.714	664.751	5	-0.1	35.76
SKIGSTENLK-VQIINKK-a2-b6	TAU_HUMAN P10636-8	TAU_HUMAN P10636-8	xlink	intra-protein xl	259	280	21	2055.194	514.806	4	-0.2	34.96
IGSLDNITHVPGGGNKK-KLDLSNVQSK-a16-b1	TAU_HUMAN P10636-8	TAU_HUMAN P10636-8	xlink	intra-protein xl	369	281	88	2974.609	595.93	5	0.2	33.69
DNIKHVPGGGSVQIVYKPVDLSK-LDLSNVQSKCGSK-a4-b9	TAU_HUMAN P10636-8	TAU_HUMAN P10636-8	xlink	intra-protein xl	298	290	8	4022.12	1006.538	4	1.3	32.07
HVPGGGSVQIVYKPVDLSK-SKIGSTENLK-a13-b2	TAU_HUMAN P10636-8	TAU_HUMAN P10636-8	xlink	intra-protein xl	311	259	52	3192.744	799.194	4	1.3	31.17
HVPGGGSVQIVYKPVDLSK-VQIINKK-a13-b6	TAU_HUMAN P10636-8	TAU_HUMAN P10636-8	xlink	intra-protein xl	311	280	31	2958.688	592.745	5	-0.9	31.16
VTSKCGSLGNIHHKPGGGQVEVK-VQSKIGSLDNITHVPGGGNK-a4-b4	TAU_HUMAN P10636-8	TAU_HUMAN P10636-8	xlink	intra-protein xl	321	353	32	4546.36	1137.598	4	-2.4	30.73
HVPGGGSVQIVYKPVDLSK-KLDLSNVQSK-a13-b1	TAU_HUMAN P10636-8	TAU_HUMAN P10636-8	xlink	intra-protein xl	311	281	30	3247.787	812.954	4	1.5	30.46
IGSLDNITHVPGGGNKK-VQIINKK-a16-b6	TAU_HUMAN P10636-8	TAU_HUMAN P10636-8	xlink	intra-protein xl	369	280	89	2685.514	538.111	5	-1.5	29.47
DNIKHVPGGGSVQIVYKPVDLSK-SKIGSTENLK-a4-b2	TAU_HUMAN P10636-8	TAU_HUMAN P10636-8	xlink	intra-protein xl	298	259	39	3662.989	1222.004	3	0.2	28.37
DNIKHVPGGGSVQIVYKPVDLSK-SEKLDFK-a4-b3	TAU_HUMAN P10636-8	TAU_HUMAN P10636-8	xlink	intra-protein xl	298	343	45	3452.857	864.222	4	0.5	27.78
VQSKIGSLDNITHVPGGGNK-LDLSNVQSKCGSK-a4-b9	TAU_HUMAN P10636-8	TAU_HUMAN P10636-8	xlink	intra-protein xl	353	290	63	3592.846	1198.623	3	-1.5	26.51
HVPGGGSVQIVYKPVDLSK-LDLSNVQSKCGSK-a13-b9	TAU_HUMAN P10636-8	TAU_HUMAN P10636-8	xlink	intra-protein xl	311	290	21	3551.869	888.975	4	0.9	26.46
VQSKIGSLDNITHVPGGGNK-HVPGGGSVQIVYKPVDLSK-a4-b13	TAU_HUMAN P10636-8	TAU_HUMAN P10636-8	xlink	intra-protein xl	353	311	42	4137.225	690.545	6	0.6	26.33
HVPGGGSVQIVYKPVDLSKVTSK-LDFKDR-a19-b4	TAU_HUMAN P10636-8	TAU_HUMAN P10636-8	xlink	intra-protein xl	317	347	30	3324.813	665.97	5	1.4	26.12
HQPGGGKVQIINK-SKIGSTENLK-a7-b2	TAU_HUMAN P10636-8	TAU_HUMAN P10636-8	xlink	intra-protein xl	274	259	15	2588.429	648.115	4	0.1	25.97
HQPGGGKVQIINK-SEKLDFK-a7-b3	TAU_HUMAN P10636-8	TAU_HUMAN P10636-8	xlink	intra-protein xl	274	343	69	2378.297	793.774	3	0.6	25.62
HVPGGGSVQIVYKPVDLSKVTSK-SEKLDFK-a19-b3	TAU_HUMAN P10636-8	TAU_HUMAN P10636-8	xlink	intra-protein xl	317	343	26	3397.851	680.578	5	0.4	23.85
VQSKIGSLDNITHVPGGGNK-HQPGGGKVQIINK-a4-b7	TAU_HUMAN P10636-8	TAU_HUMAN P10636-8	xlink	intra-protein xl	353	274	79	3532.912	884.236	4	0.1	20.45
CGSLGNIHHKPGGGQVEVK-SEKLDFKDR-a10-b7	TAU_HUMAN P10636-8	TAU_HUMAN P10636-8	xlink	intra-protein xl	331	347	16	3247.644	812.919	4	0.8	19.62
VTSKCGSLGNIHHKPGGGQVEVK-HVPGGGSVQIVYKPVDLSK-a4-b13	TAU_HUMAN P10636-8	TAU_HUMAN P10636-8	xlink	intra-protein xl	321	311	10	4505.405	902.089	5	4.3	19.37
DNIKHVPGGGSVQIVYKPVDLSK-VTSKCGSLGNIHHKPGGGQVEVK-a4-b4	TAU_HUMAN P10636-8	TAU_HUMAN P10636-8	xlink	intra-protein xl	298	321	23	4975.638	830.281	6	0.8	18.29
HVPGGGSVQIVYKPVDLSK-IGSLDNITHVPGGGNKK-a13-b16	TAU_HUMAN P10636-8	TAU_HUMAN P10636-8	xlink	intra-protein xl	311	369	58	3823.072	1275.365	3	2.2	17.1
HVPGGGSVQIVYKPVDLSKVTSK-KLDLSNVQSK-a19-b1	TAU_HUMAN P10636-8	TAU_HUMAN P10636-8	xlink	intra-protein xl	317	281	36	3663.029	733.614	5	1.1	16.89
DNIKHVPGGGSVQIVYKPVDLSK-IGSTENLKHQPGGGK-a4-b8	TAU_HUMAN P10636-8	TAU_HUMAN P10636-8	xlink	intra-protein xl	298	267	31	4109.194	822.847	5	0.8	16.16
LDLSNVQSKCGSKDNIK-TKIATPR-a9-b2	TAU_HUMAN P10636-8	TAU_HUMAN P10636-8	xlink	intra-protein xl	290	150	140	2828.497	566.707	5	-3.5	15.32
HVPGGGSVQIVYKPVDLSK-IGSTENLKHQPGGGK-a13-b8	TAU_HUMAN P10636-8	TAU_HUMAN P10636-8	xlink	intra-protein xl	311	267	44	3638.949	1213.991	3	1.8	15.02
DNIKHVPGGGSVQIVYKPVDLSK-TPPAPKTPPSSGEPPX-a4-b6	TAU_HUMAN P10636-8	TAU_HUMAN P10636-8	xlink	intra-protein xl	298	180	118	4288.26	1073.073	4	-3.4	14.61
VTSKCGSLGNIHHKPGGGQVEVK-KAKGADGK-a14-b1	TAU_HUMAN P10636-8	TAU_HUMAN P10636-8	xlink	intra-protein xl	331	141	190	3299.727	825.939	4	-4.3	12.01
IGSTENLKHQPGGGK-LDLSNVQSKCGSK-a8-b9	TAU_HUMAN P10636-8	TAU_HUMAN P10636-8	xlink	intra-protein xl	267	290	23	3094.573	774.651	4	0.3	10.99
HVPGGGSVQIVYKPVDLSKVTSK-CGSLGNIHHKPGGGQVEVK-a19-b10	TAU_HUMAN P10636-8	TAU_HUMAN P10636-8	xlink	intra-protein xl	317	331	14	4505.388	751.906	6	0.5	10.52
VQIINKKLDLSNVQSK-IGSTENLKHQPGGGK-a6-b8	TAU_HUMAN P10636-8	TAU_HUMAN P10636-8	xlink	intra-protein xl	280	267	13	3485.904	1162.976	3	-4.9	10.29
HVPGGGSVQIVYKPVDLSKVTSK-SKIGSTENLK-a19-b2	TAU_HUMAN P10636-8	TAU_HUMAN P10636-8	xlink	intra-protein xl	317	259	58	3607.99	903.005	4	1.9	9.73
SKDGTGSDDK-EPKKVAVVR-a2-b4	TAU_HUMAN P10636-8	TAU_HUMAN P10636-8	xlink	intra-protein xl	132	225	93	2171.15	724.724	3	3	9.46
IGSTENLKHQPGGGK-SEKLDFK-a8-b3	TAU_HUMAN P10636-8	TAU_HUMAN P10636-8	xlink	intra-protein xl	267	343	76	2525.302	632.333	4	-4	9.22
IETHKLTFRENAX-TPPKSPSSAX-a5-b4	TAU_HUMAN P10636-8	TAU_HUMAN P10636-8	xlink	intra-protein xl	375	234	141	2950.552	591.118	5	0.1	8.95
IETHKLTFR-MVSKSK-a5-b4	TAU_HUMAN P10636-8	TAU_HUMAN P10636-8	xlink	intra-protein xl	375	130	245	1960.09	654.371	3	4.3	8.94
IPAKTPPAPKTPPSSGEPPX-LDFKDRVQSK-a10-b4	TAU_HUMAN P10636-8	TAU_HUMAN P10636-8	xlink	intra-protein xl	180	347	167	3482.866	871.724	4	-3.3	8.37
AKGADGKTK-CGSKDNIK-a7-b4	TAU_HUMAN P10636-8	TAU_HUMAN P10636-8	xlink	intra-protein xl	148	294	146	1932.999	645.341	3	2.6	8.06

Pulse Sonication XL-MS Data

Id	Protein1	Protein2	Type	XLType	AbsPos1	AbsPos2	deltaAA	Mr	Mz	z	Error_rel[ppm]	Id-Score
IGSTENLKHQPGGGK-KLDLSNVQSK-a8-b1	TAU_HUMAN P10636-8	TAU_HUMAN P10636-8	xlink	intra-protein xl	267	281	14	2790.491	698.631	4	1.3	33.22
HQPGGGKVQIINK-SKIGSTENLK-a7-b2	TAU_HUMAN P10636-8	TAU_HUMAN P10636-8	xlink	intra-protein xl	274	259	15	2588.429	648.115	4	0.3	29.67
IGSTENLKHQPGGGK-VQIINKK-a8-b6	TAU_HUMAN P10636-8	TAU_HUMAN P10636-8	xlink	intra-protein xl	267	280	13	2501.4	626.358	4	1.4	28.05
IGSLDNITHVPGGGNKK-SEKLDFKDR-a16-b3	TAU_HUMAN P10636-8	TAU_HUMAN P10636-8	xlink	intra-protein xl	369	343	26	2980.565	746.149	4	1.1	19.72
GADGKTK-MVSKSX-a5-b4	TAU_HUMAN P10636-8	TAU_HUMAN P10636-8	xlink	intra-protein xl	148	130	18	1605.846	536.29	3	4	12.83
KIETHXLTFR-TPPKSPSSAX-a1-b4	TAU_HUMAN P10636-8	TAU_HUMAN P10636-8	xlink	intra-protein xl	370	234	136	2636.423	879.816	3	-2	7.52
AKTDHGAEIVYK-MVSKSK-a2-b4	TAU_HUMAN P10636-8	TAU_HUMAN P10636-8	xlink	intra-protein xl	385	130	255	2147.123	716.716	3	-3.1	6.87
SKDGTGSDDK-EPKKVAVVR-a2-b3	TAU_HUMAN P10636-8	TAU_HUMAN P10636-8	xlink	intra-protein xl	132	224	92	2171.151	724.725	3	3.5	6.7
AKTDHGAEIVYK-GADGKTXIATPR-a2-b5	TAU_HUMAN P10636-8	TAU_HUMAN P10636-8	xlink	intra-protein xl	385	148	237	2796.48	933.168	3	1.2	6.05
SKIGSTENLX-TKIATPR-a2-b2	TAU_HUMAN P10636-8	TAU_HUMAN P10636-8	xlink	intra-protein xl	259	150	109	2113.167	705.397	3	-3.4	5.95
KLDLSNVQSXCGSK-AKGADGXTK-a1-b2	TAU_HUMAN P10636-8	TAU_HUMAN P10636-8	xlink	intra-protein xl	281	143	138	2803.453	935.492	3	1	5.93

Mechanical Homogenization and Pulse Sonication XL-MS Data

Id	Protein1	Protein2	Type	XLType	AbsPos1	AbsPos2	deltaAA	Mr	Mz	z	Error_rel[ppm]	Id-Score
CGSKDNIK-ENAKAX-a4-b4	TAU_HUMAN P10636-8	TAU_HUMAN P10636-8	xlink	intra-protein xl	294	383	89	1831.91	458.985	4	-0.1	15.8
KLDLSNVQSKCGSK-KVAVVR-a10-b1	TAU_HUMAN P10636-8	TAU_HUMAN P10636-8	xlink	intra-protein xl	290	225	65	2371.325	593.839	4	-0.2	15.51
TPPSSGEPPKSGDR-IPAKTPPAPK-a10-b4	TAU_HUMAN P10636-8	TAU_HUMAN P10636-8	xlink	intra-protein xl	190	174	16	2567.36	642.848	4	0.1	14.08
SRLQTAPVPMPDLKNVX-SKDGTGSDDKK-a14-b2	TAU_HUMAN P10636-8	TAU_HUMAN P10636-8	xlink	intra-protein xl	254	132	122	3281.677	657.343	5	-4.6	13.49
DGTGSDDKX-KIETHX-a8-b1	TAU_HUMAN P10636-8	TAU_HUMAN P10636-8	xlink	intra-protein xl	140	370	230	2041.988	681.67	3	-2	10.3
KLDLSNVQSK-TKIATPR-a1-b2	TAU_HUMAN P10636-8	TAU_HUMAN P10636-8	xlink	intra-protein xl	281	150	131	2054.177	685.734	3	1.9	9.84
SEKLDFX-VQIINKX-a3-b6	TAU_HUMAN P10636-8	TAU_HUMAN P10636-8	xlink	intra-protein xl	343	280	63	2073.148	692.057	3	0.3	9.57
SKDGTGSDDK-LDFKDR-a2-b4	TAU_HUMAN P10636-8	TAU_HUMAN P10636-8	xlink	intra-protein xl	132	347	215	1938.919	647.314	3	1.2	9.01